Thesis

Thermodynamic Theory of the Glass Transition of Binary Mixtures of Disparate Size Ratio
二成分系のサイズ比が大きく離れた系におけるガラス転移の熱力学理論

Harukuni Ikeda

Division of Material Science (Physics)
Graduate School of Science
Nagoya University

March 27, 2017

Contents

1 Introduction **5**

1.1 Viscosity and relaxation time 5

1.1.1 Angel plot 5

1.1.2 Dynamical correlation functions and relaxation time . . 6

1.2 Experimental glass transition point and Kauzman transition point 8

1.3 The configurational entropy and the Kauzman transition . . . 11

1.4 Static correlation function of the glass transition 13

1.5 Cage effect 14

1.6 The glass transition of binary mixtures of disparate size ratio . 15

2 Mode-coupling theory and replica liquid theory **18**

2.1 The mode-coupling theory (MCT) 19

2.2 A mean-field scenario of the glass transition 20

2.2.1 Configurational entropy and Kauzman transition . . . 21

2.2.2 Adam-Gibbs theory 22

2.2.3 The Monasson's method 23

2.2.4 Benchmark test of the Manasson's method: Static properties of the p-spin spherical model 24

2.2.5 Dynamic properties of the p-spin spherical model and the MCT transition temperature 26

2.3 Replica liquid theory 30

2.4 Other theories of the glass transition 34

2.4.1 Random-first order phase transition theory (RFOT) . . 34

2.4.2 Dynamical facilitation theory 35

2.5 Summary 37

3 Spin glass model for the glass transition of binary mixtures 39
3.1 Introduction . . . 40
3.2 Model . . . 42
3.3 Free energy calculation . . . 43
3.3.1 1RSB ansatz . . . 43
3.3.2 2RSB ansatz . . . 45
3.3.3 Numerical minimization of G_{2RSB} . . . 46
3.4 Phase diagrams and thermodynamic quantities . . . 46
3.4.1 Order parameters and phase diagrams . . . 47
3.4.2 Thermodynamic quantities . . . 54
3.5 Discussion . . . 56
3.5.1 Connection to the randamly pinned PSM . . . 56
3.5.2 Connection to the MCT of binary mixtures . . . 57
3.6 Conclusions . . . 59

4 Replica liquid theory for binary mixtures of disparate size ratio 61
4.1 Introduction . . . 61
4.2 Model . . . 63
4.3 1RSB Ansatz . . . 64
4.4 2RSB Ansatz . . . 65
4.5 Thermodynamic phase diagram . . . 67
4.6 Configurational entropy . . . 69
4.7 Summary and discussion . . . 71

5 A paradox of the replica liquid theory of binary mixtures in the one-component limit 72
5.1 Introduction . . . 72
5.2 Theory . . . 74
5.3 Conclusion . . . 77

6 Conclusion 78

A Perturbation analysis of the continuous transition 81

B 1RSB thermodynamic phase diagram 85

C Derivation of eq. (4.3) 88

D Dynamical phase diagram **90**

Chapter 1

Introduction

This thesis is devoted to development of the thermodynamic aspects of the glass transition of multi-component mixtures. In a most broad sense, the glasses are amorphous materials which are frozen without any crystalline order and do not flow at least on the experimental time scale [1–6]. The glasses are ubiquitous in our daily life and very common material in industries. However, the nature of the glasses is still not yet fully understood. In this chapter, we explain the physics of the glass transition and introduce several important quantities to characterize the glass transition.

1.1 Viscosity and relaxation time

When the temperature of liquids changes sufficiently slow, liquids turn into crystals at the melting point. However, when the temperature is changed so fast to avoid the crystallization, the system becomes the supercooled liquid state. As the temperature is decreased further, the viscosity of the supercooled liquids increases very rapidly and eventually the system is frozen in amorphous configuration at some temperature. This is the so-called glass transition [1, 2, 4, 5].

1.1.1 Angel plot

The glass transition is observed for many kinds of liquids including the molecular liquids, polymer, and colloids [1,2]. In Fig. 1.1, we show the temperature dependence of the viscosity of the various glass forming liquids [1, 7, 8]. Since

the temperature range within which the dramatic slowing down is observed differ significantly for different materials, we have introduced the re-scaled temperature, T_g/T. Conventionally, T_g is selected as the temperature at which viscosity reaches $\eta(T_g) = 10^{15}$ poise since the relaxation time of the supercooled liquids becomes compatible with the experimental time scale, $10^2 - 10^3$ sec, at this temperature. The plot with the re-scaled temperature T_g/T is referred to as the Angel plot [1,8,9]. In Fig. 1.1, some glassy material such as SiO_2 and GeO_2 exhibit the well-known Arrhenius law like growth of the viscosity:

$$\log \eta \propto 1/T. \tag{1.1}$$

This means that the activation energy for rearrangement of the constituent particles is temperature independent and the viscosity becomes zero only at $T = 0$. There is no signature of the phase transition at finite temperature. The supercooled liquid whose viscosity is well fitted by eq. (1.1) is referred to as the *strong* glass. Much interesting cases are such as m, o-Xylene and o-Terphenyl whose viscosity exhibit much stronger temperature dependence than that expected by eq. (1.1). Those glassy materials are referred to as the *fragile* glass former [1, 2, 4]. The rapid increase of the viscosity of fragile glasses implies the underlying phase transition. The viscosity of the fragile glasses is well fitted by the Voger-Fulcher-Tammann (VFT) equation [10]:

$$\log \eta \propto \frac{1}{T - T_0}. \tag{1.2}$$

The VFT law means that the viscosity diverges at the finite temperature and suggests the existence of the genuine phase transition at $T = T_0$.

1.1.2 Dynamical correlation functions and relaxation time

As the viscosity increases, the motion of constituent particles of supercooled liquids dramatically slows down. To characterize this phenomenon, one would observe the density-density correlation function [11]:

$$F(k,t) = \frac{1}{N} \sum_{i<j}^{N} \left\langle e^{i\boldsymbol{k}\cdot(\boldsymbol{x}_i(t) - \boldsymbol{x}_i(0))} \right\rangle, \tag{1.3}$$

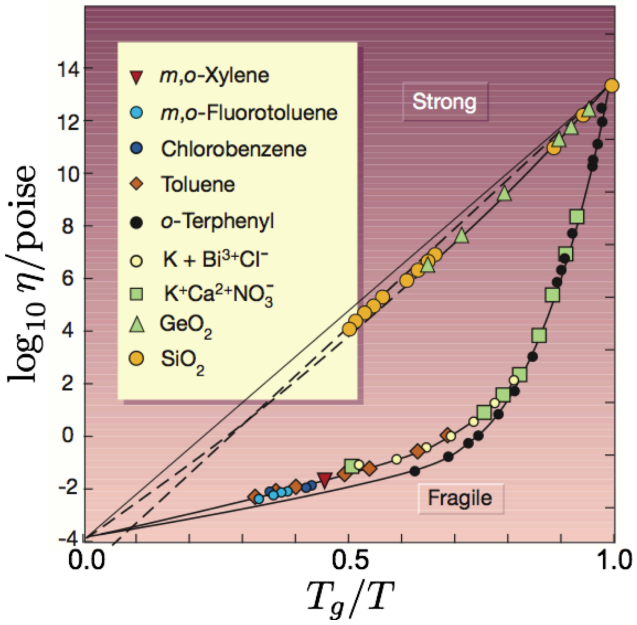

Figure 1.1: The viscosity of various supercooled liquids (Angel plot): The picture has been taken from Ref. [1].

where N denotes the number of the particles and $\boldsymbol{x}_i(t)$ denotes the position of the i-th particle at time t. about As the temperature is decreased, the relaxation time of $F(k,t)$, τ_α, dramatically increases. η and τ_α are connected by the Maxwell relation [2, 11]:

$$\eta = G_\infty \tau_\alpha, \tag{1.4}$$

where G_∞ is the infinite frequency shear modulus. In many cases, the temperature dependence of G_∞ is much weaker than that of τ_α. One can consider that η is proportional to τ_α and the two quantities have qualitatively the same temperature dependence. In particular, τ_α can be well approximated by the same functional form of the viscosity, eq. (1.2):

$$\log \tau_\alpha \propto \frac{1}{T - T_0}. \tag{1.5}$$

Hereafter, we mainly discuss τ_α instead of η since it is more convenient to treat than that of η from the theoretical point of view.

1.2 Experimental glass transition point and Kauzman transition point

As mentioned in the previous section, the relaxation time, τ_α, dramatically increases in the proximity of T_0 (see eq. (1.5)) and τ_α exceeds the observation time at a certain temperature, T_g higher than T_0, and constituent particles freeze within the observation time scale. This is the experimental glass transition and T_g is referred to as the experimental glass transition point [1, 5]. The observed specific heat changes discontinuously at T_g since the translational degree of freedoms of the constituent particles are not observed below T_g. Concomitantly, the entropy, which is the integral of the specific heat, exhibits a kink at T_g.

As it is clear from this definition, T_g depends on the observation time. If one waits longer time, the transition point may shift to lower temperature. This is schematically shown in Fig. 1.2, where T_{g1} and T_{g2} denote the experimental glass transition temperatures with shorter and longer observation time, respectively. The longer observation time, the lower glass transition point one obtains. The question is what would happen if the observation time is infinity. Does T_g keep decreasing down to zero temperature? Or

is there any terminal point below which T_g stops decreasing? There is an interesting argument by Kauzman [1, 2]; In general, the specific heat of the supercooled liquid is larger than that of the crystal due to the contribution from the translational degree of freedom of constituent particles. It means that the entropy of the supercooled liquid decreases faster than that of the crystal as shown in Fig. 1.2. In other words, the entropy of the supercooled liquid becomes lower than that of the crystal below a certain temperature. However, it is unlikely that disordered configurations like liquids have the lower entropy than that of the ordered configurations like crystals. This is the so-called Kauzman's paradox and the temperature at which the entropy of supercooled liquid coincides with that of the crystal is referred to as the Kauzman point, T_K [1, 2]. To avoid this paradoxical situation, the translational degree of freedom of the supercooled liquid must be frozen at or above T_K since it is the origin of the steeper temperature dependence of the supercooled liquid. In other words, the particles must be frozen in an amorphous configuration. This phenomenon is the so-called *ideal* glass transition or Kauzman transition.

The existence of the Kauzman transition is still actively debated. First of all, no one can reach the Kauzman point since the relaxation time increases very rapidly and overcomes the observation time before reach the Kauzman point. Second, it is possible that the temperature dependence of the supercooled liquids becomes gradually milder with decreasing the temperature. In this case, there is, at best, just a crossover from the supercooled liquid state to the glass state. Last but not least, there is no guarantee that disordered configurations like liquid have the higher entropy than that of ordered configurations like crystals. Note, only the fact that the ground state of the one-component hard spheres is the face-centered cubic (FCC) structure has been proved very recently [12–14]. Besides this simplest case, we do not know the exact ground state and cannot exclude the possibility that the disordered configuration might be the grand state.

Aside from such a subtle problem, if one accepts the existence of the Kauzman transition, an interesting question is whether or not T_K coincides with the dynamically defined glass transition point, T_0, in eq. (1.5). We will discuss this point in detail in the next section.

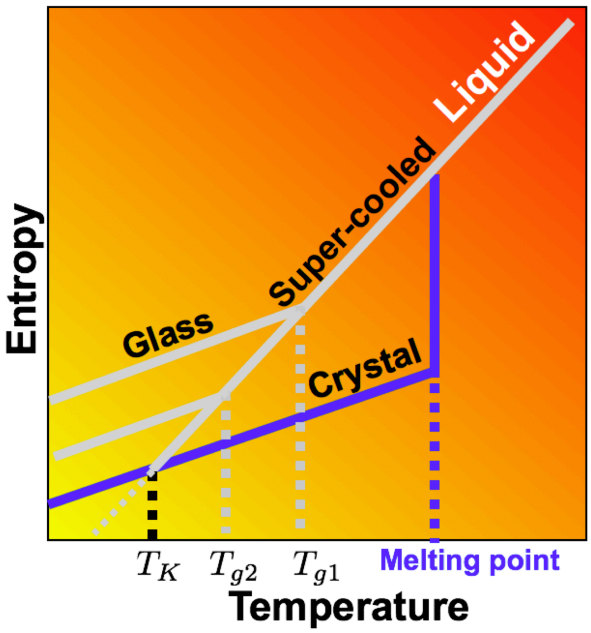

Figure 1.2: The schematic picture of the temperature dependence of the entropy of supercooled liquids: T_{g1} and T_{g2} denote the glass transition point obtained by the fast and slow quench, respectively. T_K denotes the Kauzman transition point at which the entropy of the supercooled liquids coincides with that of the crystal.

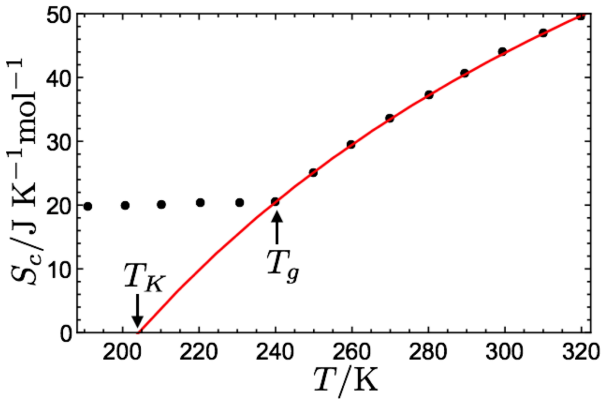

Figure 1.3: The configurational entropy of *O*-terphenyl: The filled circles denote the experimental data. The solid line is the result of fitting. The date has been taken from Ref. [15].

1.3 The configurational entropy and the Kauzman transition

Here, we shall continue to discuss the Kauzman transition in more detail. As explained in the previous section, the Kauzman transition is defined as the temperature where the entropy of the supercooled liquid coincides with that of the crystal. The difference between the entropy of the supercooled liquid, S_{liq}, and the entropy of the crystal, S_{cry}, is referred to as the configurational entropy:

$$S_c \equiv S_{liq} - S_{cry}. \tag{1.6}$$

As an example, in Fig. 1.3, we show the temperature dependence of S_c of *O*-terphenyl [15], which is a typical fragile glass former as shown in Fig. 1.1. S_c can be well fitted by the following function:

$$S_c(T) = S_\infty(1 - T_K/T), \tag{1.7}$$

where $S_\infty = 137.4$ J K^{-1} mol^{-1} and $T_K = 242$ K. Note that at $T = T_g \approx 246$ K, the relaxation time exceeds the observation time ($\approx 10^2$ s) and thus the data below T_g not be equilibrated. Interestingly, the Kauzman transition temperature, T_K, obtained by the fitting, eq. (1.7), is very close to the glass transition point obtained by the VFT fitting of the relaxation time,

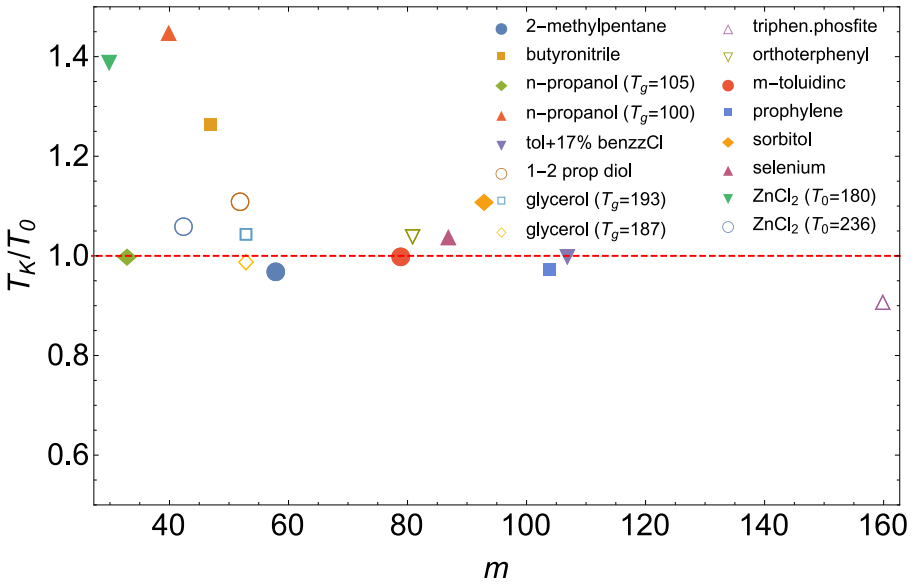

Figure 1.4: The fragility dependence of T_K/T_0 for various glassy materials: T_K is the Kauzman temperature where the configurational entropy vanishes. T_0 is the putative (dynamical) glass transition point where the relaxation time diverges. m is the fragility index. The data has been taken from Ref. [15].

$T_0 = 202.4$ K [15], at which the relaxation time becomes infinite. In Fig. 1.4, we have plotted T_K/T_0 for various glassy materials as a function of the fragility index $m \equiv \left(\frac{\partial \log_{10}\eta}{\partial(T_g/T)}\right)_{T=T_g}$, namely, the steepness of the temperature dependence of η. The more fragile glasses have the large value of m. The figure demonstrates that

$$T_0 = T_K \tag{1.8}$$

holds at least approximately for the fragile liquid, say, $m > 80$. Note, T_0 is deduced from the dynamical quantity like the viscosity and relaxation time while T_K is deduced from the thermodynamic quantity like the configurational entropy. Eq. (1.8) claims that those apparently different temperatures are coincides. This is a highly nontrivial relation and this open the way to construct the thermodynamic theory of the glass transition which we shall discuss in the next chapter.

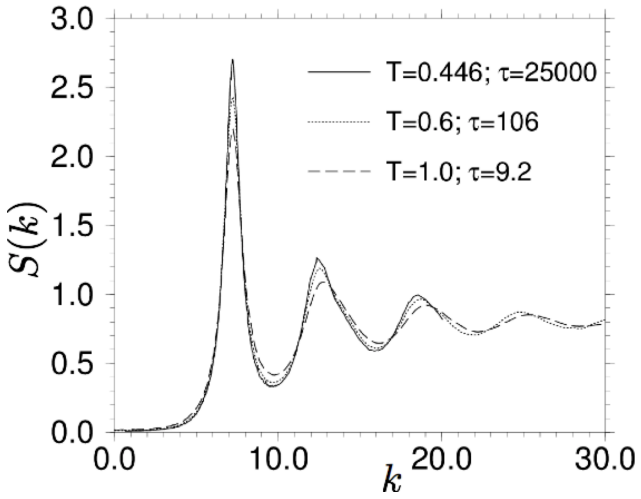

Figure 1.5: Static structure factor of the Lennerd-Joned mixtures. The solid line denotes the data at $T = 0.446$ where the relaxation time is $\tau = 25000$. The dotted line denotes the data at $T = 0.6$ where the relaxation time is $\tau = 106$. The dashed line denotes the data at $T = 1.0$ where the relaxation time is $\tau = 9.2$. The plot has been taken from Ref. [16]

1.4 Static correlation function of the glass transition

As mentioned before, the supercooled liquids exhibit dramatic slowing down while those configurations are almost indistinguishable from the high temperature normal liquids. Here we explain this point more detail.

One of the most commonly observed quantities to characterize the configuration of the liquid is the density-density correlation function. Its Fourier transformation is called the static structure factor, $S(k)$ [11]. $S(k)$ is defined as

$$S(k) = \frac{1}{N} \sum_{ij=1}^{N} \left\langle e^{i\boldsymbol{k}\cdot(\boldsymbol{x}_i - \boldsymbol{x}_j)} \right\rangle , \tag{1.9}$$

where N denotes the number of constituent particles, $\boldsymbol{k}$ denotes the wave vector and $\boldsymbol{x}_i$ denotes the position of the i-th particle. For isotropic systems, $S(k)$ does not depend on the direction of $\boldsymbol{k}$ and is a function of $k = |\boldsymbol{k}|$.

It is well established that the fluctuation of the order parameter is significantly enhanced near the critical point. In usual critical phenomena like gas-liquid transition, this fluctuation also appears on $S(k)$. The pronounced peak at small k grows with approaching the critical point. However, this is not the case of the glass transition [17,18]. In Fig. 1.5, we show that $S(k)$ for several temperatures. τ's in the legends are the relaxation times evaluated by the time dependent density-density correlation function. One observes that $S(k)$ is almost temperature independent whereas the relaxation time increases over several orders of magnitude [16]. This is because the supercooled liquids have the almost same structure and symmetry that of high temperature liquids. This is in marked contrast to the conventional critical phenomena where the transition is accompanied with the structure change and is well characterized by $S(k)$.

1.5 Cage effect

Although the static properties of the supercooled liquid are insensitive to the temperature change, its dynamical properties significantly change with decreasing the temperature. The low temperature supercooled liquid exhibits solid like behavior in the time scale shorter than the relaxation time. This is the so-called cage effect. Here, we briefly review this.

As mentioned before, one of the most commonly used quantities to characterize the dynamics of the supercooled liquid is the time dependence density-density correlation function, $F(k,t)$, which is defined by eq. (1.3) [1, 11]. In Fig. 1.6, we show the typical behavior of $F(k,t)$ [1]. The vertical axis is normalized so as to become unity at $t = 0$. At the sufficiently high temperature, $F(k,t)$ quickly decays to zero as usual liquids. As the temperature decreases, the relaxation time of $F(k,t)$ dramatically increases. Furthermore, $F(k,t)$ develops intermediate plateau and shows two step decay. The plateau of $F(k,t)$ implies that the particle does not move very much for long time. This is because the particle motion is hindered by the particles surrounding the particle. This is the cage-effect. The situation is similar to that of the lattice vibration of crystals where the constituent particles oscillate around their equilibrium positions [20].

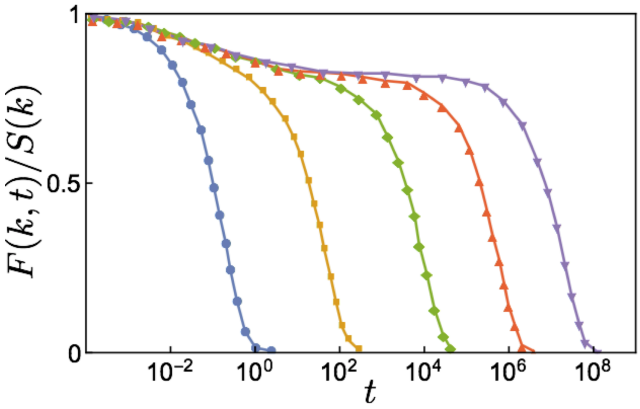

Figure 1.6: The normalized dynamical structure factor of the Lenard-Jones mixtures: The wave number is chosen as $k = 7.1$. The temperature decreases from left to right from $T = 3.0$ to 0.8975. The data has been taken from Ref. [19].

1.6 The glass transition of binary mixtures of disparate size ratio

So far, most theoretical studies have been focused on the glass transition of one-component systems consisting of spherical particles [21, 22]. However, in many cases, the systems are multi-component mixtures and consists of non-spherical particles, and exhibit much richer behavior than that of the idealized one-component system consisting of spherical particles. In particular, we would like to focus on the decoupling of the glass transition points. In Fig. 1.7, we show the examples of the decoupling phenomena. Fig. 1.7 (a) describes the binary mixtures consisting of large and small particles. When the size ratio between large and small particles is much larger than unity, the glass transition points of large and small particles are decoupled [23–26]. In other words, there arises the phase where only large particles are vitrified while small particles remain liquid. Fig. 1.7 (b) describes the system consisting of elliptical particles (or, in general, non-spherical particles). In this case, one should take into account the degrees of freedom of the rotational and translational degree of freedoms. When the aspect ratio is much larger than unity, the glass transition points of the translational and rotational degree of freedoms can be decoupled [27, 28]. Fig. 1.7 (c) denotes the ionic

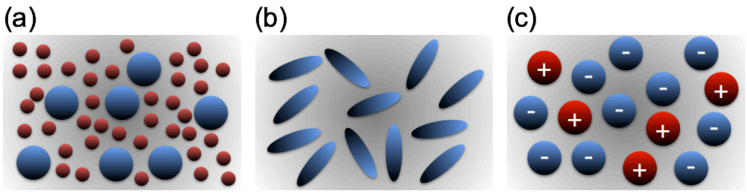

Figure 1.7: Examples of the decoupling phenomena: (a) The binary mixture consisting of large and small particles. When the size ratio between the large and small particles is much larger than unity, the glass transition points of large and small particles can be decoupled. (b) The system consisting of elliptical particles. When the aspect ratio is much large than unity, the glass transition points of the rotational and translational degree of freedoms can be decoupled. (c) The ionic system. The glass transition points of anions and cations can be decoupled.

system. The glass transition points of anions and cations can be decoupled depending on the atomic numbers of those atoms [29–32].

In this thesis, we will focus on the glass transition of binary mixtures of the disparate size ratio since we believe that this is the simplest system to study the decoupling phenomenon. In Fig. 1.8, we show the phase diagram obtained by the experiment of the system consisting of large and small colloidal particles. Since colloidal particles approximately behave as hard spheres, the relevant control parameter is the packing fraction rather than the temperature [11]. In Fig. 1.8, the horizontal axis denotes the packing fraction of large colloids, φ_L, and the vertical axis denotes the packing fraction of small colloids, φ_S. There are two kinds of district glass phases on the phase diagram. In the glass phase indicated by the blue unfilled squares in Fig. 1.8, both large and small particles are vitrified. The other glass phase is denoted by the black unfilled squares in Fig. 1.8 where only large particles are vitrified while small particles remain as liquid. The glass transition points of large and small particles are decoupled. We construct a thermodynamic theory to describe this decoupling phenomena.

The contents of rest of the chapters are following. In Chapter 2, we first explain the current mean-field theory of the glass transition which has been developed to describe the glass transition of the one-component or nearly one-component systems. In Chapter 3, we investigate the binary extension of the p-spin spherical model (PSM). The PSM is one of the paradigmatic

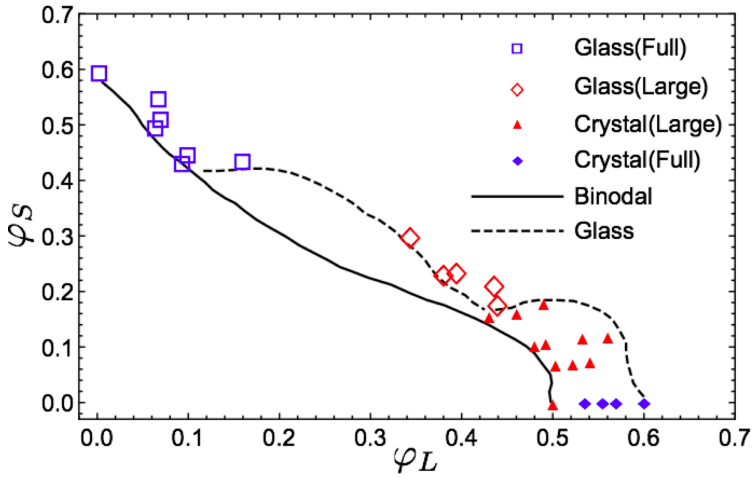

Figure 1.8: The phase diagram of the colloidal system consisting of large and small particles. The blue unfilled squares denote the phase where both large and small particles are vitrified. The black unfilled diamonds denote the phase where only the large particle are vitrified while the small particles are liquid. The red filled triangles denote the phase where only the large particles are crystallized while small particle are fluid. The gray filled diamonds denote the perfect crystal. The black solid line denotes the binodal curve of the liquid and crystal. The dotted line indicates the glass transition line. The plot is taken from Ref. [23].

mean-field model of the glass transition and can be solved analytically. The investigation of the binary PSM reveals that the free energy landscape of the binary mixtures of the disparate size ratio has more complex free energy landscape than that of the one component system. With above observation in mind, in Chapter 4, we investigate the more realistic particle system which mimics the binary colloidal system consisting of large and small particles. We calculate the phase diagram of the model in the high dimensional limit where analytical treatment is available and show that the resultant phase diagram is qualitatively the same with the result obtained by the colloidal experiment (Fig. 1.8). Along the way to investigate the binary mixtures, we found that the theory of binary mixture is *inconsistent* with the theory of one-component system. In Chapter 5, we discuss how this inconsistency is resolved.

Chapter 2

Mode-coupling theory and replica liquid theory

In this chapter, we review the two theoretical frameworks of the glass transition of one-component systems. One is the mode-coupling theory (MCT) [3, 33]. The MCT predicts the dynamics of the density correlation function from the first principles calculation and well reproduces the experimental and simulation results at moderately high temperature. However, it is unlikely that the MCT gives the complete understanding of the glass transition since it has several crucial problems. The MCT relies on the uncontrollable and unjustified approximations. Furthermore, the MCT predicts the spurious non-ergodic transition at higher than the experimental glass transition temperature. Thus, the MCT breaks down at low temperature. An alternative framework that resolves above problems has been proposed, which is the so-called replica liquid theory (RLT) [21, 22]. The advantages of the RLT are followings. (1) There exist several controllable approximation schemes. In particular, it is known that the theory becomes exact in the high dimensional limit (mean-field limit). (2) The theory predicts the genuine thermodynamic transition point where the relaxation time diverges. (3) The theory gives a physical interpretation of the MCT transition point. In the rest of sections, we first briefly describe the MCT and then, give a rather detailed explanation of the RLT.

2.1 The mode-coupling theory (MCT)

The MCT predicts the time evolution of the density correlation function,

$$F(k,t) = \frac{1}{N}\sum_{i<j}^{N} \left\langle e^{i\boldsymbol{k}\cdot(\boldsymbol{x}_i(t)-\boldsymbol{x}_j(0))} \right\rangle, \tag{2.1}$$

where N denotes the number of the particles and the three dimensional vector $\boldsymbol{x}_i(t)$ denotes the position of the i-th particles at time t. According to the MCT, $F(k,t)$ is determined by the following self-consistent integrodifferential equation:

$$\frac{\partial^2 F(k,t)}{\partial t^2} + \Gamma_k \frac{\partial F(k,t)}{\partial t} + \Omega_k^2 F(k,t) = -\int_0^t dt' \Omega_k^2 M(k,t-t') \frac{\partial F(k,t')}{\partial t'}, \tag{2.2}$$

where $\Omega_k^2 = k_B T k^2/mS(k)$ and Γ_k is a constant related to the short time dynamics and not related to the long time dynamics. The memory kernel is given by

$$M(k,t) = \frac{S(k)}{2\rho}\int \frac{d\boldsymbol{q}}{(2\pi)^3} V_k^2(\boldsymbol{q}, \boldsymbol{k}-\boldsymbol{q}) F(k-q,t) F(q,t), \tag{2.3}$$

where the vertex function is defined as

$$V_k(\boldsymbol{q}_1, \boldsymbol{q}_2) \equiv \rho \left\{ \boldsymbol{k}\cdot\boldsymbol{q}_1 C(q_1) + \boldsymbol{k}\cdot q_2 C(q_2) \right\}. \tag{2.4}$$

$S(k)$ is the static structure factor and $C(k)$ is the direct correlation function [11]. The MCT equation, eq. (2.2), reproduces some important properties of the glass transition such as the two step relaxation of the density correlation function and the rapid increase of the relaxation time. In particular, the MCT predicts that the relaxation time diverges toward the MCT transition temperature T_{MCT} as

$$\tau_\alpha \propto (T - T_{MCT})^{-\gamma}, \tag{2.5}$$

where γ is the material dependent constant. This power law increase of τ_α is indeed observed for the supercooled liquids at moderately high temperature. In Fig. 2.1, we show the relaxation time of the *o*-terphenyl with the MCT fit,

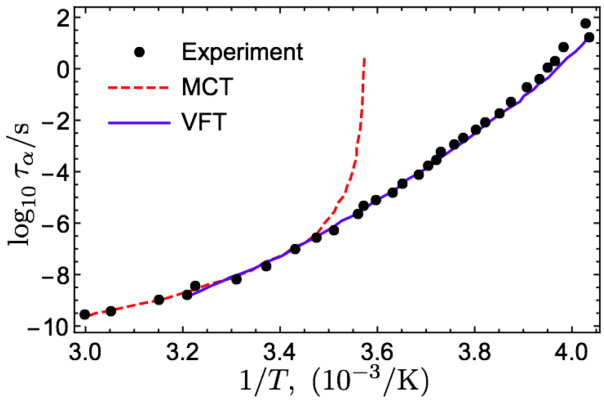

Figure 2.1: The relaxation time of *o*-terphenyl: The filled circles denote the relaxation time of the *o*-terphenyl obtained by the experiment. The red dashed line denotes the MCT fit. The blue solid line denotes the VFT fit. The data has been taken from Ref. [6].

eq. (2.5) [6,34]. One observes that MCT fit works well at higher temperature than $T_{MCT} \approx 285$K.

Despite of the success of the MCT at high temperature, the MCT breaks down at low temperature as shown in Fig. 2.1. The relaxation time of the supercooled liquids remains finite even below T_{MCT} whereas the MCT predicts that it becomes infinite. Below T_{MCT}, the relaxation time is well fitted by the Voger-Fulcher-Tammann (VFT) law:

$$\log \tau_\alpha \propto \frac{1}{T - T_0}, \tag{2.6}$$

see the blue solid line in Fig. 2.1. Describing the supercooled liquids below T_{MCT} is clearly out of range of the MCT. The replica liquid theory resolves this problem.

2.2 A mean-field scenario of the glass transition

The replica liquid theory is constructed based on the mean-field scenario (MFS) of the glass transition. Before explain the replica liquid theory, we first describe the MFS in this section. The MFS is the scenario inspired

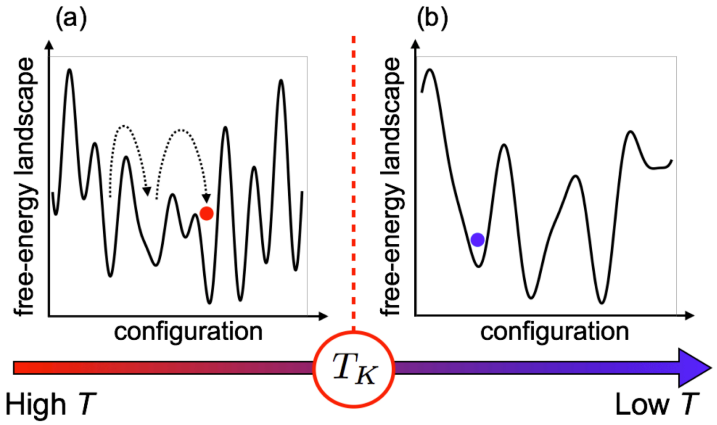

Figure 2.2: The schematic picture of the free-energy landscape: (a) The free-energy landscape above the Kauzman transition temperature, T_K. There are exponentially many minima on the free-energy. The system can earn the entropy by traveling around different minima. (b) The free-energy landscape below T_K. The number of minima is sub-exponentially and does not contribute to the entropy in the thermodynamic limit. Since, the system cannot earn the entropy by traveling around different minima, the system is trapped in a minimum.

by the similarity between the supercooled liquid and some mean-field spin glass models [35–37]. The MFS gives the physical interpretation of the two important temperatures of the glass transition mentioned before, the mode-coupling transition temperature, T_{MCT}, and the Kauzman transition point, T_K. In the framework of the MFS, the Kauzman transition at T_K is identified with the one-step replica symmetry breaking (1RSB) transition which is first discovered in a class of the mean-field spin-glass models [35, 36]. Contrary, the MCT transition at T_{MCT} is identified with the spinodal point at which the metastable-states of the glass disappear [35]. In this section, we first describe the physical meaning of T_K and then, describe how the crossover at T_{MCT} is interpreted in the framework of the MFS.

2.2.1 Configurational entropy and Kauzman transition

The basic assumption is that the slow dynamics of supercooled liquids is caused by the complex structure of the free-energy landscape, see Fig. 2.2

[35–37]. For the intermediate time scale, the system might be trapped in a minimum of the free-energy. The driving force to escape from the minimum is the configurational entropy:

$$\Sigma \equiv S_{liq} - S_{viv}, \tag{2.7}$$

where S_{liq} is the entropy of the liquid and S_{viv} is the vibrational entropy in the minima. At sufficiently high temperature, $\Sigma > 0$ and the system can obtain the entropy by visiting the many metastable states, see Fig. 2.2 (a). With decreasing the temperature, Σ decreases and eventually vanishes at a certain temperature, T_K. The driving force to escape from a minimum vanishes and the system would be trapped in the minimum forever, see Fig. 2.2 (b). This is the Kauzman transition.

To evaluate Σ, we rely following two assumptions. (i) The vibrational entropy is compatible with the entropy of the crystal. With this assumption, eq. (2.7) can be written as

$$\Sigma \approx S_{liq} - S_{cry}, \tag{2.8}$$

where S_{cry} is the entropy of the crystal. Eq. (2.8) is the same with that has been introduced in the introduction, see eq. (1.6). (ii) We neglect the correlation between the different minima of the free-energy. With this assumption, Σ is interpreted as the logarithm of the number of minima of the free-energy landscape,

$$\Sigma \approx k_B \log N_c, \tag{2.9}$$

where N_c is the number of the minima and k_B is the Boltman's constant. In the next few sections, we examine the connection between the relaxation time and Σ, and how to theoretically calculate N_c and Σ.

2.2.2 Adam-Gibbs theory

The Adam-Gibbs theory (AGT) is a phenomenological theory which successfully relates the relaxation time to the configurational entropy [2,37,38]. The main assumption of the AGT is that the system is divided into N/n number of sub-systems containing n particles. The sub-system, which is referred to as the corporative rearranging region (CRR), can take small number of configurations, say, Ω. The total number of rearrangements of the entire system

is $N_c = \Omega^{N/n}$, which might be corresponds to the number of minima of the free-energy in Fig. 2.2. The configurational entropy is the logarithm of the number of the minima (see eq. (2.9)):

$$\Sigma(T) = k_B \log \Omega^{N/n}. \tag{2.10}$$

To discuss the behavior of the relaxation time, we rely on the Arrenius formula:

$$\tau_\alpha = \tau_0 e^{\Delta F/k_B T}, \tag{2.11}$$

where τ_0 is a temperature independent constant and ΔF is the free-energy cost to change the configuration of the CRR. It is natural to guess that ΔF is proportional to the size of the CRR, $\Delta F \propto n$. Using eq. (2.10), n can be expressed in terms of $\Sigma(T)$ as

$$n = \frac{k_B \log \Omega}{\Sigma(T)}. \tag{2.12}$$

With those assumptions, the relaxation time can be calculated as

$$\tau_\alpha = \tau_0 \exp\left[\frac{C \log \Omega}{T\Sigma(T)}\right], \tag{2.13}$$

where C is a constant. This equation is the main consequence of the AGT, which relates the relaxation time, τ_α, to the configurational entropy, $\Sigma(T)$. In the next sub-section, we will discuss the theoretical framework to evaluate Σ.

2.2.3 The Monasson's method

It is believed that the free-energy landscape of the supercooled liquids at sufficiently low temperature has exponentially many number of metastable states separated by the high energy barriers [2,4,22,37]. We assume that the partition function is expressed by the summation of the contribution from each metastable states:

$$Z = \sum_\alpha e^{-\beta N f_\alpha} = \int df e^{-\beta N f + \Sigma(f)}, \tag{2.14}$$

where $\Sigma(f) = \sum_\alpha \delta(f - f_\alpha)$ is nothing but the configurational entropy. Monasson has invented an elegant way to calculate the configurational entropy [39]. The main idea is to introduce the m replicas of the original system. The partition function of the replicated system is

$$\begin{aligned} Z_m &= \sum_\alpha e^{-\beta N m f_\alpha} \\ &= \int df e^{-\beta N m f + \Sigma(f)} \\ &\approx e^{-\beta N m f^*(T) + \Sigma(f^*(T))}, \end{aligned} \tag{2.15}$$

where $f^*(T)$ is determined by the saddle point condition:

$$\frac{\partial}{\partial f}\left(-\beta N m f + \Sigma(f)\right) = 0. \tag{2.16}$$

From eq. (2.15), one can show that

$$\frac{\partial}{\partial m} \log Z_m = -\beta N f^*(T) \tag{2.17}$$

and

$$\Sigma(f^*(T)) = \log Z_m - m \frac{\partial}{\partial m} \log Z_m. \tag{2.18}$$

Thus, once the partition function of the m replica system is obtained, one can evaluate the configurational entropy by eq. (2.18).

2.2.4 Benchmark test of the Manasson's method: Static properties of the p-spin spherical model

Here we review the p-spin spherical model (PSM) which is a fully connected spin-glass model and shows the glass like slow dynamics [40–43]. Since the model can be solved analytically, it is an ideal model to benchmark the Monasson's method. We shall consider the spin model which interact with the following p-body potential:

$$H = \sum_{i_1 < i_2 < \cdots < i_p}^{N} J_{ijk} \sigma_i \sigma_j \sigma_k, \tag{2.19}$$

where $\sigma_i \in (-\infty, \infty)$ with a spherical constraint, $\sum_{i=1}^{N} \sigma_i^2 = N$. N is the number of spins and J_{ijk} is the random variable whose distribution function is

$$P(J) \propto \exp\left[-\frac{N^2}{p!}J^2\right]. \tag{2.20}$$

Following the Manasson's method, we shall introduce m replicas. The partition function of the replicated system for the given set of the quenched randomness, $\boldsymbol{J} = \{J_{ijk}\}_{1\le i<j<k\le N}$, is

$$Z_m[\boldsymbol{J}] = \prod_{a=1}^{m}\left(\prod_{i=1}^{N}\int_{-\infty}^{\infty} d\sigma_i^a\right)\delta(N - \sum_{i=1}^{N}(\sigma_i^a)^2)\exp\left[-\beta\sum_{a=1}^{m}\sum_{i<j<k} J_{ijk}\sigma_i^a\sigma_j^a\sigma_k^a\right]. \tag{2.21}$$

The self-averaging property allows one to estimate the free-energy as

$$\log Z_m[\boldsymbol{J}] \approx \overline{\log Z_m[\boldsymbol{J}]}, \tag{2.22}$$

where the overline denotes the average over the quenched randomness $\boldsymbol{J}$. To evaluate eq.(2.22), we replace the quenched average by the annealed one:

$$\overline{\log Z_m[\boldsymbol{J}]} \approx \log \overline{Z_m[\boldsymbol{J}]}. \tag{2.23}$$

Then, the partition function can be calculated as

$$\begin{aligned}
\overline{Z_m[\boldsymbol{J}]} &= \mathrm{Tr}\exp\left[\frac{N\beta^2}{4}\sum_{ab=1}^{m}\left(\frac{1}{N}\sum_{i=1}^{N}\sigma_i^a\sigma_i^b\right)^p\right], \\
&= \int DQ_{ab}D\lambda_{ab}\exp\left[\frac{N\beta^2}{4}\sum_{ab}Q_{ab}^p + \sum_{ab}\lambda_{ab}\left(NQ_{ab} - \sum_i \sigma_i^a\sigma_i^b\right)\right] \\
&\approx e^{NS(Q)},
\end{aligned} \tag{2.24}$$

where we have introduced the effective action:

$$S(Q) = \frac{\beta^2}{4}\sum_{ab}Q_{ab}^p + \frac{1}{2}\log\det Q_{ab}. \tag{2.25}$$

Q_{ab} is the saddle point value of $\sum_i \sigma_i^a\sigma^b/N$. The remaining task is to optimize eq. (2.25) for Q_{ab}. However, the full optimization for completely general Q_{ab}

is extremely difficult and one should assume some ansatz. The standard one is

$$Q_{ab} = (1-q)\delta_{ab} + q, \tag{2.26}$$

where δ_{ab} is the Kronecker delta. This is the so-called one-step replica symmetry breaking (1RSB) ansatz. Substituting eq. (2.26) into the free-energy, eq. (2.25), one obtains

$$S(Q_{ab}) = m(m-1)\frac{\beta^2}{4}q^p + \frac{m-1}{2}\log(1-q) + \frac{1}{2}\log(1-(1-m)q). \tag{2.27}$$

q is determined so as to optimize S. This saddle point condition, $\partial_q S = 0$, can be explicitly written as

$$\frac{q}{1-q} = \frac{pJ^2}{4}q^p. \tag{2.28}$$

Substituting eq. (2.27) into eq. (2.18), one finally obtains the configurational entropy. The direct calculation leads to

$$\Sigma(T) = -\frac{\beta^2}{4}q^p - \frac{1}{2}\log(1-q) - \frac{1}{2}q. \tag{2.29}$$

The temperature dependence of the configurational entropy calculated by eq. (2.29) is plotted in Fig. 2.3. Note that at $T > T_d = \sqrt{3/8} \approx 0.612$, $\Sigma(T)$ becomes imaginary and cannot be defined. It means that at $T > T_d$, the free-energy minima are not well defined and one cannot count the number of the minima. We discuss this point in more detail in the next subsection. Below T_d, $\Sigma(T)$ monotonically decreases with decreasing the temperature, and eventually vanishes at $T_K \approx 0.585$. This is the signature of the Kauzman transition. Near T_K, $\Sigma(T)$ can be expanded as

$$\Sigma(T) \approx C(T_K)(T - T_K), \tag{2.30}$$

where $C(T_K)$ is the specific heat at T_K. Remarkably, substituting eq. (2.30) into the AG equation, eq. (2.13), one can reproduce the VFT low, eq. (1.2).

2.2.5 Dynamic properties of the p-spin spherical model and the MCT transition temperature

As well as the static properties, there are lots of works have been done to investigate the dynamical property of the PSM [42,43]. Here we briefly sketch

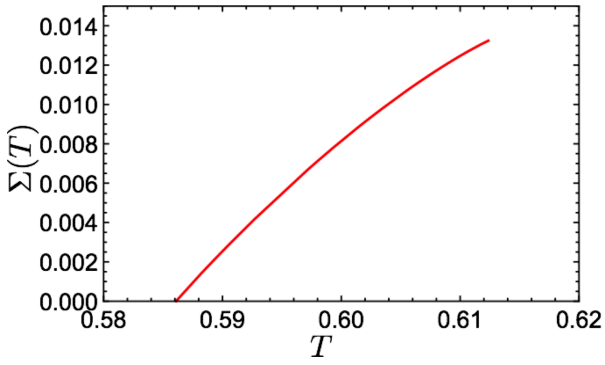

Figure 2.3: The configurational entropy of the PSM: The configurational entropy decreases with the temperature and vanishes at $T_K \approx 0.585$ at which the thermodynamic glass transition takes place.

the results which give us the physical interpretation of the MCT transition temperature, T_{MCT}.

It is known that the dynamics of the supercooled liquids at sufficiently long time scale is independent from the detailed of the rule of the time evolution. For instance, the newtonian dynamics, Langevin dynamics, and Monte carlo algorithm give the same result [44, 45]. This allows us to select a suitable rule for the theoretical treatment. Here, we consider the Langevin dynamics:

$$\frac{\partial \sigma_i(t)}{\partial t} = -\mu(t)\sigma_i(t) - \frac{\partial H}{\partial \sigma_i} + \eta_i(t), \tag{2.31}$$

where $\mu(t)$ is the Lagrange multiplier to enforce the spherical constraint, $\sum_{i=1}^{N} \sigma_i(t)^2 = N$. We assume that the thermal noise, $\eta_i(t)$ is the white Gaussian noise whose variance is

$$\langle \eta_i(t)\eta_j(t')\rangle = 2T\delta_{ij}\delta(t-t'). \tag{2.32}$$

The model can be analyzed by the Martin-Siggia-Rose formalism [46]. After some manipulations, one reaches the closed equation of the equilibrium time correlation function, $C(t) = \sum_{i=1}^{N} \langle \sigma_i(t)\sigma_i(0)\rangle / N$ [42, 43]:

$$\frac{\partial C(t)}{\partial t} = -TC(t) - \frac{p}{2T}\int_0^t dt' C^{p-1}(t-t')\frac{\partial C(t')}{\partial t'}. \tag{2.33}$$

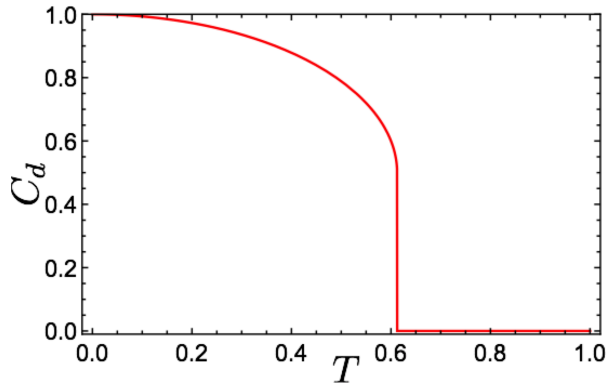

Figure 2.4: The temperature dependence of C_d: C_d changes discontinuously at $T_d = \sqrt{3/8} \approx 0.61$ from zero to a finite value.

Quite interestingly, the mathematical structure of the above equation is the same with that of the mode coupling theory (MCT), see eq.(2.2) [11, 33].

Eq. (2.33) can be investigated though the Laplace transformation. In particular, the value of the correlation function in the long time limit can be calculated by solving following self-consistent equation:

$$\frac{C_d}{1 - C_d} = \frac{p}{2T^2} C_d^{p-1}, \tag{2.34}$$

where we have defined

$$C_d \equiv \lim_{t \to \infty} C(t). \tag{2.35}$$

The temperature dependence of C_d obtained by solving eq. (2.34) for $p = 3$ is shown in Fig. 2.4. At sufficiently high temperature, $C_d = 0$ meaning that the correlation function $C(t)$ decays to zero in the long time limit. C_d changes discontinuously at $T_d = \sqrt{3/8} \approx 0.61$ from zero to a finite value. When $T < T_d$, the correlation function does not decay to zero even in the long time limit and the ergodicity is broken. Note, T_d is *higher* than the Kauzman transition point, $T_K \approx 0.585$ at which the genuine thermodynamic glass transition takes place. Instead, T_d is the temperature above which Σ becomes imaginary number (see Fig. 2.3).

The above strange result is now interpreted as an artifact of the mean-field model. It has been shown that T_d is the spinodal point of the metastable

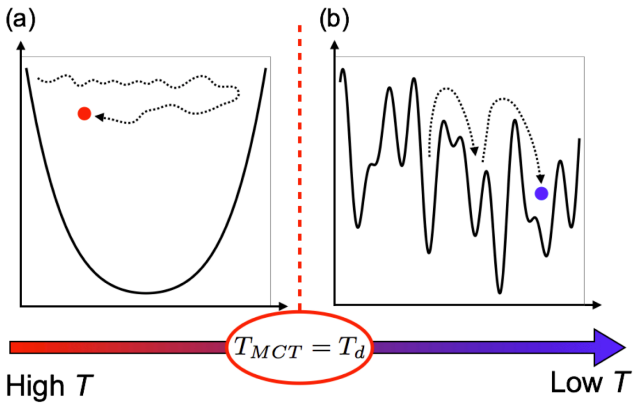

Figure 2.5: Schematic pictures of the free-energy landscape: (a) The free-energy landscape above T_{MCT}. The free-energy has only one minimum and the system can travel around the entire phase space without crossing the energy barrier. (b) The free-energy landscape below T_{MCT}. There are many number of minima on the free-energy separated by the high energy barriers. The system must overcome the energy barrier to move from a minimum to another minimum.

glass states [43]. When $T < T_d$, there are many minima on the free-energy each of which corresponds to a metastable glass state, while when $T > T_d$, there are no minima on the free-energy, see Fig. 2.5. Since the PSM is a mean-field model, the free-energy barriers between the minima are infinitely large in the thermodynamic limit, $N \to \infty$. The system is trapped in a minimum and the relaxation time diverges at $T = T_d$. Note that the state that the system is trapped in a minimum is just a metastable state and the thermodynamic quantities does not show any singularities.

Since the MCT equation, eq. (2.2), and the dynamical equation of the PSM, eq. (2.33), are very similar, we expect that the phenomenology of the supercooled liquids at T_{MCT} is similar to that of the PSM at T_d. This conjecture has been proved quite recently for the mean-field model: one-component hard spheres in the high dimensional limit [47,48]. To justify this conjecture for more realistic models in finite dimensions, we shall observe the

eigen values of the Hessian matrix [49, 50]:

$$H_{nm} \equiv \sum_{i<j} \nabla_n \nabla_m v(\boldsymbol{x}_i - \boldsymbol{x}_j), \tag{2.36}$$

where $v(\boldsymbol{x}_i - \boldsymbol{x}_j)$ denotes the interaction potential between the i-th and j-th particles and $\boldsymbol{x}_i$ denotes the position of the i-th particle. Diagonalizaing the Hessian matrix at the saddle point [1], one can count the number of the negative modes of the eigenvalues, n_s, and calculate the fraction of the negative saddles, $n_s/3N$. The result for the Lennard-Jones mixtures, which is a typical model system of the glass transition, is shown in Fig. 2.6. When $T > T_{MCT}$, the fraction of the negative modes is finite. The system can travel around the phase space through the negative directions without crossing the free-energy barrier. This is the same situation of that described in Fig. 2.5 (a). With decreasing the temperature, the fraction of the negative modes decreases and becomes zero at T_{MCT}. Below T_{MCT}, all modes of the Hessian matrix is positive meaning that there are many number of minima on the free-energy separated by the high energy barriers. The system should overcome the free-energy barrier to travel around the phase space. Again, this is the same situation of that described in Fig. 2.5 (b). Unlike the PSM, the free-energy barrier between the minima of the supercooled liquid (at finite dimension) is finite. Thus, the system can escape from a minimum in a finite amount of time. The driving force within this temperature range is the configurational entropy and the relaxation time is described by the VFT law, eq. (2.6).

2.3 Replica liquid theory

Based on the mean-field scenario described in the previous section, Mezard *et al.* have constructed the first principle theory of the glass transition which allows to calculate the quantitative values of several thermodynamics quantities such as the configurational entropy and the Kauzman transition point [21,22]. The theory is referred to as the replica liquid theory (RLT). There are several approximation schemes are proposed. Among them, we explain the effective potential method (EPM) since it is the quantitatively most successful theory and shown to be exact at the high dimensional limit [22].

[1] The saddle point is the configuration, $\{\boldsymbol{x}_i\}_{i=1,\cdots,N}$, where $\sum_{i<j} \nabla_j v(\boldsymbol{x}_i - \boldsymbol{x}_j) = 0$.

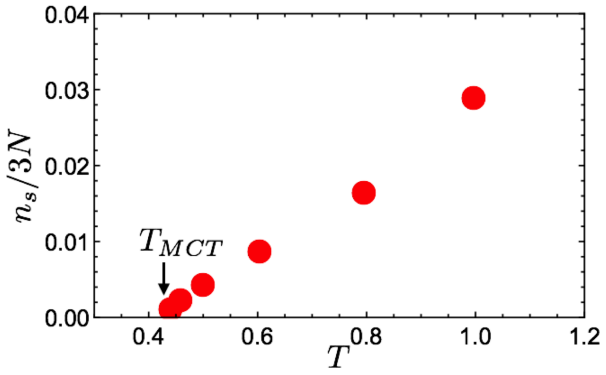

Figure 2.6: The fraction of the negative saddles of the Lennard-Jones mixture: The fraction of the negative saddles vanishes at $T_{MCT} \approx 0.435$. The data have been taken from Ref. [50].

As for the spin-glass models, the staring point is the partition function of the m replicated system:

$$Z_m = \sum_{N=0}^{\infty} \frac{1}{N!} \prod_{a=1}^{m} \prod_{i=1}^{N} \int d\boldsymbol{x}_i^a \exp\left[-\beta \sum_{a=1}^{m} \sum_{i<j} v(\boldsymbol{x}_i^a - \boldsymbol{x}_j^a) - \beta \sum_{i=1}^{N} \psi(\boldsymbol{x}_i^1, \cdots, \boldsymbol{x}_i^m) \right], \tag{2.37}$$

where the d-dimensional vector $\boldsymbol{x}_i^a$ denotes the position of the i-th particle of the a-th replica and $v(\boldsymbol{r})$ denotes the pair interaction potential. We have introduced the external potential, $\psi(\boldsymbol{x}^1, \cdots, \boldsymbol{x}^m)$, which reinforces that the m replicas are trapped in a same basin[2]. ψ is conjugated to the density distribution function of the replica space:

$$\rho(\overline{\boldsymbol{x}}) = \sum_{i=1}^{N} \left\langle \prod_{a=1}^{m} \delta(\boldsymbol{x}_i^a - \boldsymbol{x}^a) \right\rangle = -\frac{1}{\beta} \frac{\delta \log Z_m[\psi(\overline{\boldsymbol{x}})]}{\delta \psi(\overline{\boldsymbol{x}})}, \tag{2.38}$$

where we introduced the abbreviated notation, $\overline{\boldsymbol{x}} = \{\boldsymbol{x}^1, \cdots, \boldsymbol{x}^m\}$. Taking the Legendre transformation from $\psi(\overline{x})$ to $\rho(\overline{x})$, one obtains the free-energy functional of $\rho(\overline{\boldsymbol{x}})$:

$$-\beta F_m[\rho(\overline{\boldsymbol{x}})] = \log Z_m[\psi] - \int d\overline{\boldsymbol{x}} \psi(\overline{\boldsymbol{x}}) \rho(\overline{\boldsymbol{x}}). \tag{2.39}$$

[2]Note that because of this external potential, the m replicas are not independent, thus the Gibbs factor is $N!$ rather than $N!^m$.

Following the standard method of the liquid theory [11], F_m can be divided as follow:

$$-\beta F_m[\rho(\overline{\boldsymbol{x}})] = \int \rho(\overline{\boldsymbol{x}})(1 - \log \rho(\overline{\boldsymbol{x}})) - \beta F_{ex}[\rho(\overline{\boldsymbol{x}})], \tag{2.40}$$

where the first term is the free-energy of the ideal gas and the second term is the contribution of the particle interactions. Using the Mayer cluster expansion, F_{ex} can be expanded as

$$-\beta F_{ex}[\rho(\overline{\boldsymbol{x}})] = \frac{1}{2} \int d\overline{\boldsymbol{x}} d\overline{\boldsymbol{y}} \rho(\overline{\boldsymbol{x}}) \rho(\overline{\boldsymbol{y}}) f(\overline{\boldsymbol{x}} - \overline{\boldsymbol{y}}) + O(\rho^3), \tag{2.41}$$

where

$$f(\overline{\boldsymbol{x}} - \overline{\boldsymbol{y}}) = \prod_{a=1}^{m} e^{-\beta v(x^a - y^a)} - 1 \tag{2.42}$$

is the Mayer function in the replica space. Once F_m is obtained, the configurational entropy is estimated by the following formula:

$$\Sigma(T) = \lim_{m \to 1} \left[m^2 \frac{\partial}{\partial m} \left(\frac{\beta F_m}{m} \right) \right]. \tag{2.43}$$

Furthermore, the density distribution function, $\rho(\overline{\boldsymbol{x}})$, allows us to calculate the cage size:

$$A = \frac{2}{m(m-1)} \sum_{a<b} \sum_{i=1}^{N} \left\langle \left(\boldsymbol{x}_i^a - \boldsymbol{x}_i^b \right)^2 \right\rangle = \frac{2}{m(m-1)} \sum_{a<b} \int d\overline{\boldsymbol{x}} \rho(\overline{\boldsymbol{x}}) \left(\boldsymbol{x}^a - \boldsymbol{x}^b \right)^2. \tag{2.44}$$

The cage size, A, plays the role of the order parameter to distinguish the glass and liquid. In the glass phase, A has a finite value while in the liquid phase, A becomes infinite.

One of the advantages of the effective potential method EPM compared to the MCT is that the approximation is under control: It is shown that the EPM gives the exact result in the high dimensional limit, $d \to \infty$ [22]. In this limit, the higher order terms than the second order expansion become negligible. Thus, the free-energy functional is reduced to

$$-\beta F_m[\rho(\overline{\boldsymbol{x}})] = \int d\overline{\boldsymbol{x}} \rho(\overline{\boldsymbol{x}})(1 - \log \rho(\overline{\boldsymbol{x}})) + \frac{1}{2} \int d\overline{\boldsymbol{x}} d\overline{\boldsymbol{y}} \rho(\overline{\boldsymbol{x}}) \rho(\overline{\boldsymbol{y}}) f(\overline{\boldsymbol{x}} - \overline{\boldsymbol{y}}). \tag{2.45}$$

The free-energy is obtained by optimizing above equation. However, it is a hard tasks to optimize for completely general density profile, $\rho(\overline{\boldsymbol{x}})$. Thus, we assume the following Gaussian Ansatz:

$$\rho(\overline{\boldsymbol{x}}) = \rho \int d\boldsymbol{X} \prod_{a=1}^{m} \gamma_A(\boldsymbol{x}^a - \boldsymbol{X}) \tag{2.46}$$

with

$$\gamma_A(\boldsymbol{r}) = \frac{1}{(2\pi A)^{d/2}} e^{-r^2/2A}. \tag{2.47}$$

Substituting eq. (2.46) into the free-energy functional, eq. (2.45), one obtains

$$-\beta \frac{F(A,m)}{N} = 1 - \log\rho + S_H(A) + \frac{\rho}{2} \int d\boldsymbol{r}\,(q(\boldsymbol{r}) - 1) \tag{2.48}$$

with

$$\begin{aligned} S_H(A) &= \frac{d}{2}(m-1)\log(2\pi A) - \frac{d}{2}(1 - m - \log m), \\ q(\boldsymbol{r}) &= \int d\boldsymbol{u} \gamma_{2A}(\boldsymbol{u} + \boldsymbol{r}) e^{-\beta v(\boldsymbol{u})}. \end{aligned} \tag{2.49}$$

The cage size A is to be determined by the saddle point condition:

$$\frac{1}{A} = \frac{\rho}{d(1-m)} \frac{\partial}{\partial A} \int d\boldsymbol{r} q(\boldsymbol{r})^m \tag{2.50}$$

For the hard sphere system, the dynamical transition point, where eq. (2.50) begins to have non-trivial solution, can be calculated as

$$\varphi_d \approx 4.8 d 2^{-d}. \tag{2.51}$$

The asymptotic form of the configurational entropy in the high dimensional limit is

$$\Sigma(\varphi) = \frac{1}{2}\left(d\log d - \varphi\right). \tag{2.52}$$

The Kauzman transition point is obtained by $\Sigma(\varphi_K) = 0$ as

$$\varphi_K = d\log d. \tag{2.53}$$

Apart from the mean-field limit ($d \to \infty$), one should rely on the approximation schemes of the liquid theory [11]. One of the most quantitatively reliable approximation is the so-called Carnanhan-Starling approximation (CS) [11]. For the one-component hard sphere system in three dimension, for instance, the EPM with the CS approximation gives $\varphi_K \approx 0.62$, which is reasonably close to the glass transition point reported by the numerical simulations and experiments [22].

2.4 Other theories of the glass transition

So far, we have mainly explained the mode-coupling theory (MCT) and the replica liquid theory (RLT). Those are, to our knowledge, only the *first principle* theories of the glass transition and allow one to calculate several physical quantities from the microscopic interactions between the constituent particles. It is relatively transparent to extend those theory to binary mixtures.

However, the RLT and MCT are not only the theory of the glass transition. There are other *phenomenological* theories which explain the qualitative natures of the glass transition. In this section, we shall briefly overview those for reader's convenience. But, we will not enter the detailed of the theories since those lack the microscopic justifications and we do not know how to extend those to binary mixtures.

2.4.1 Random-first order phase transition theory (RFOT)

The mode-coupling theory (MCT) and replica liquid theory (RLT) are mean-field theories in nature in a sense that the theory assume spatially uniform relaxation and do not take into account the fluctuations. However, the relaxation of supercooled liquids is far from uniform. In Fig. 2.7, we show the spatial displacements of a two dimensional supercooled liquid near the glass transition point [6]. One can observes that the displacement of particles are distributed spatially heterogeneously. This is the so-called dynamical heterogeneity and observed for many fragile glasses [51–56]. Interestingly, the typical length scale of the heterogeneous region increases with decreasing the temperature [53, 54, 57].

The random-first order phase transition theory (RFOT), which was originally proposed by Kirkpatrick, Thirumalai and Wolyness [36], is the theory

to take into account above heterogeneous nature of the low temperature supercooled liquids. The ROFT based on the very similar idea of that of the nucleation theory of the first order phase transition theory. Consider there is a droplet of the linear size R inside of which is liquid and outside of which is glass. The free-energy difference between the before and after the creation of the droplet is

$$\Delta F(R) = \Gamma R^{\theta} - S_c R^d, \tag{2.54}$$

where the first term represents the surface tension and the second term represents the configurational entropy of the droplet. The exponent θ depends on the shape of the droplet and cannot be determined by the ROFT. $\Delta F(R)$ has the maximum at

$$R^* = \left(\frac{\theta \Gamma}{d S_c} \right)^{\frac{d}{d-\theta}}. \tag{2.55}$$

If $R < R^*$, $\Delta F(R)$ is a increasing function of R while if $R > R^*$, $\Delta F(R)$ is a decreasing function of R. Since the system evolves in the direction to lower the free-energy, if $R < R^*$, the droplet diminishes and vanishes. Contrary, if $R > R^*$, the droplet can spread throughout the entire system and the system melts. In other words, the metastable glass state whose linear size is smaller than R^* is stable due to the surface tension, Γ while the metastable glass state whose liner size is larger than R^* is unstable against the melting induced by the configuration entropy. Thus, R^* is the characteristic length of the metastable glass state. One may expect that R^* somehow relates to the typical length scale of the dynamical heterogeneity shown in Fig. 2.7. This is an interesting question, but, to be honest, the accessible temperature range in present numerical simulation and experiment is too restricted and we can not give any conclusive answer [58–61]. So, we will not discuss this problem anymore.

2.4.2 Dynamical facilitation theory

The dynamical facilitation theory (DFT) claims that the glass transition is a purely dynamical transition *without* any thermodynamic singularity [6,62]. In the DFT, one assumes that there are few number of "mobile particles" at low temperature. A mobile particle facilitates surrounding particles. This leads to a cascade process since some neighbours of the facilitated particles also

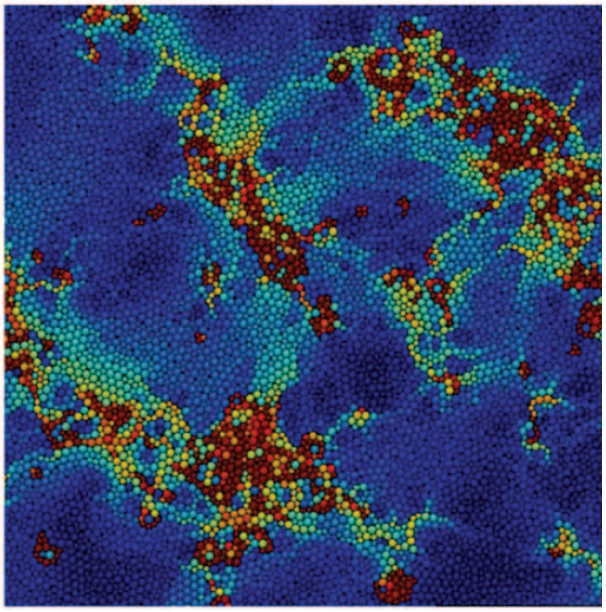

Figure 2.7: Dynamical heterogeneity obtained by the numerical simulation of a two dimensional glass former: The particles are colored according to their displacement during the time scale compatible with the relaxation time. The particles of larger displacement are shown by red while the particles of smaller displacement are shown by blue. The picture has been taken from Ref. [6].

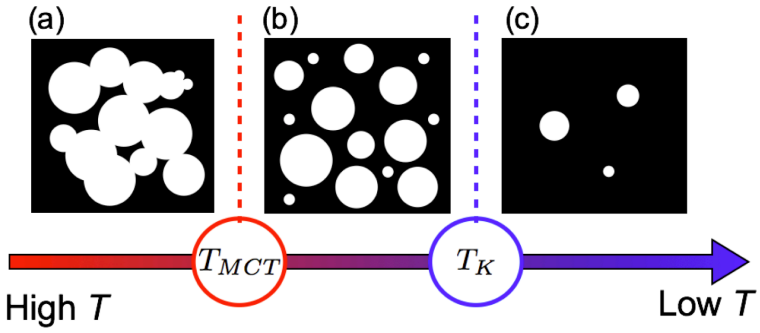

Figure 2.8: Summary of the random first order transition theory (MFS): (a) The schematic picture of the phase space structure at $T > T_{MCT}$. Accessible region of the phase space is colored in white and inaccessible region is colored in black. Note, the accessible regions are connected to each other. (b) The phase space structure at $T \in (T_K, T_{MCT})$. The accessible region splits into exponentially many metastable states. (c) The phase space structure at $T < T_K$. The number of metastable states becomes sub-exponential.

facilitate another particles and so on and so forth. Following this scenario, the DFT can explain qualitatively the dramatic increase of the relaxation time. However, the theory is still phenomenological revel and lacks the microscopic justification. For instance, there is not first principle theory to determine the "mobile particles" and how those particles facilitate another particles. In particular, we do not know how the theory is extended so as to describe the binary mixtures of disparate size ratio. This is a fascinating question, but, we left it for a future work.

2.5 Summary

In Fig. 2.8, we summarize the random-first order phase transition theory (MFS) which we have explained through this chapter. When $T > T_{MCT}$, all available areas of the phase space are connected, see Fig. 2.8 (a). The system can travel around the phase space without crossing the free-energy barriers. When $T < T_{MCT}$, there arise the exponentially many metastable states on the free-energy and the phase space splits into many sub-spaces,

see Fig. 2.8 (b). In case of the mean-field model such as the p-spin spherical model (PSM), the relaxation time diverges at T_{MCT} since the free-energy barriers between the minima become infinite and the system cannot escape from a metastable state. Contrary, in finite dimensions, the free-energy barriers between the metastable states are finite and the system is trapped in a metastable state only for a finite amount of time. The MCT transition becomes just a crossover. The main driving force blow T_{MCT}, is the configurational entropy, namely, the logarithm of the number of the minima of the free-energy. The configurational entropy decreases with decreasing the temperature and eventually vanishes at the Kauzman transition temperature, T_K. Combining the Adam-Gibbs theory and Monasson's method, one can predict $\log \tau_\alpha \propto (T - T_K)^{-1}$, which is the well-known VFT.

So far, all results have been given for one-component systems. From next chapter, we shall describe how the picture established in the one-component systems can be extended into the many-component mixtures.

Chapter 3

Spin glass model for the glass transition of binary mixtures

In order to gain insights on the glass transition of the binary mixtures of the desperate size ratio, we introduce and study a two-component version of the p-spin spherical spin glass model. We employ the replica method to calculate the free energy and the phase diagram. We show that when the strengths of the interactions of each component are not widely separated, the model has only one glass phase characterized by the conventional one-step replica symmetry breaking. However when the strengths of the interactions are well separated, the model has three glass phases depending on temperature and component ratio. One is the "single" glass phase in which only the spins of one component are frozen while the spins of the other component remain mobile. This phase is characterized by the one-step replica symmetry breaking. The second is the "double" glass phase obtained by cooling further the single glass phase, in which the spins of the remaining mobile component are also frozen. This phase is characterized by the two-step replica symmetry breaking. The third is also the "double" glass phase, which however is formed by the simultaneous freezing of the spins of both components at the same temperatures and is characterized by the one-step replica symmetry breaking. We discuss the implications of these results for the glass transitions of binary mixtures.

3.1 Introduction

The p-spin spherical model (PSM) has been playing important roles in the study of the glass transition of liquids, because it shares many common properties in dynamics and thermodynamics with glass forming liquids [2,4,40,63]. The PSM is the infinite range spin glass model in which soft spins interact through p-body interactions with random quenched couplings [43]. The dynamics of the PSM can be solved semi-analytically [40, 42, 43]. Particularly at $p = 3$, the time correlation function is known to obey the dynamical equation mathematically equivalent with the mode-coupling theory (MCT) equation of the glass transition [3, 40]. The system is ergodic at high temperature, however as temperature is decreased, the time correlation function exhibits the two step relaxation behavior and the relaxation becomes slower and slower. Eventually the relaxation time diverges and the spins get frozen, which is called the *dynamical transition*. Also the thermodynamics of the PSM can be solved semi-analytically by the replica method with the one-step replica symmetry breaking (1RSB) ansatz [41, 43]. As temperature is lowered from above, the phase space of the system in the paramagnetic state splits into many metastable glassy states exactly at the dynamical transition temperature. As the system is cooled further, the logarithm of the number of these states or the complexity, which corresponds to the configurational entropy in glass forming liquids, decreases and eventually becomes zero where the *thermodynamic glass transition* takes place. In the glass phase, the free energy of the model is dominated by the lower energy states. The similarity between the PSM and glass forming liquids has many to believe that they are in the same class of random glassy systems, at least in the mean-field limit [2, 4].

However, real glass formers often exhibit richer and more anomalous dynamical behaviors, all of which can not be captured by the PSM. In this work, we particularly focus on the "decoupling" phenomenon often observed in multi-component glass formers. This is the phenomenon in which the slowing down of the dynamics of each component occurs separately at different regions of the densities and the temperatures, hence some components are frozen into a glass state while the others remain mobile. There is a wide variety of materials showing the decoupling phenomenon, such as ionic glasses and metallic glasses [32]. The simplest example among them is presumably a binary mixture of large and small particles with disparate size ratio [23–26, 64–72]. When the size ratio is sufficiently large, it is ob-

served in experiments [23, 24] and simulations [25, 26, 69] that there are two distinct glass phases in this model: the "single" glass where only large particles are arrested while small particles are left mobile, and the "double" glass where both small and large particles are arrested. Despite of simplicity of the model, this decoupling phenomenon of binary mixtures is not fully understood theoretically. It is encouraging that the MCT can predict this behavior qualitatively [70–72]. However the MCT is derived using numerous uncontrorable approximations, which are not guaranteed to be valid for binary mixtures with disparate size ratio. Even for monodisperse systems, there is an argument whether or not the MCT is a true "mean-field theory" to describe the dynamics of the glass transition [47, 73–75]. Moreover the transition predicted by the MCT only exists in the mean-field limit and is washed away in finite dimensions [2, 4].

Can any of spin glass models qualitatively capture these rich behaviors of the glass transitions of binary mixtures? If so, analysis of such models should facilitate the study of binary mixtures because spin models can be analyzed rigorously at least in the mean-field limit. Related to this point, Crisanti and Leuzzi generalized the PSM to include two distinct energy scales of the interactions [76–79]. They considered the $s + p$-spin spherical model, where all spins interact through both s-body and p-body interactions. This model is potentially related to the glass forming liquids in which molecules are subject to two different types of interactions. They found that there is a variety of glass phases characterized by the series of replica symmetry breaking [78] and that the model exhibits rich dynamical behaviors such as three-step relaxation of the time correlation function [79]. However to the best of our knowledge, there exists no study on the spin glass model which exhibits the single and double glass transitions and the decoupling of dynamics of one of the components from the other, as observed for binary mixtures.

In this work, we extend the PSM so as to mimic binary mixtures of particles with disparate size ratio. Our model is a two component version of the PSM, which is composed of weakly interacting spins (weak spins) and strongly interacting spins (strong spins). We employ the replica theory to study the thermodynamics of the model. We found that the model has the glass phases characterized by either conventional 1RSB and the two-step replica symmetry breaking (2RSB). We show that the interplay between the 1RSB and the 2RSB solutions results in the decoupling of the glass transitions of weak spins from that of strong spins. We also show that our two component PSM is directly related to the randomly pinned PSM, which has been studied

recently [80]. Finally based on the results, we discuss the validity of the predictions of the MCT for the multiple glass phases of binary mixtures.

The organization of the paper is as follows. In Section II, we introduce the model. In Section III, we use the replica theory to express the free energy in terms of the spin glass order parameters. In Section IV, by numerical minimization of the free energy, we obtain the temperature evolutions of the order parameters, the phase diagrams, and the thermodynamic quantities of the model. In Sections V and VI, we discuss the results and conclude the work.

3.2 Model

We consider a two component version of the PSM with $p = 3$. The model is composed of N_1 spins of the component 1 and N_2 spins of the component 2, with $N = N_1 + N_2$. The spin variables for each component are denoted as $\sigma_{1,i}$ $(i = 1, \cdots, N_1)$ and $\sigma_{2,i}$ $(i = 1, \cdots, N_2)$, respectively. They obey the spherical constraints $N_1 = \sum_i \sigma_{1,i}^2$ and $N_2 = \sum_i \sigma_{2,i}^2$. The Hamiltonian of the model is

$$H = \sum_{\alpha,\beta,\gamma=1,2} \sum_{i_\alpha, j_\beta, k_\gamma} J_{i_\alpha j_\beta k_\gamma}^{(\alpha\beta\gamma)} \sigma_{\alpha,i_\alpha} \sigma_{\beta,j_\beta} \sigma_{\gamma,k_\gamma}, \tag{3.1}$$

where the greek indices are used to indicate components, the roman indices are for spins, and $J_{i_\alpha j_\beta k_\gamma}^{(\alpha\beta\gamma)}$ is the coupling constant among the three spins, which is the Gaussian random variables with zero mean. In order to render the analysis tractable, we consider the case where $J_{i_\alpha j_\beta k_\gamma}^{(\alpha\beta\gamma)}$ is characterized by only the two values, i.e.

$$\overline{(J^{(\alpha\beta\gamma)})^2} = \begin{cases} \frac{3J_1^2}{N^2} & (\alpha,\beta,\gamma) = (1,1,1), \\ \frac{3J_2^2}{N^2} & (\alpha,\beta,\gamma) \neq (1,1,1). \end{cases} \tag{3.2}$$

Here J_1 and J_2 are the typical energy scales of the interactions of the component 1 and 2, respectively. We set $J_1 > J_2$, hence the component 1 is "strong" spins and 2 is "weak" spins. The control parameters of the model are the ratio of the strengths of the interactions $J = J_2/J_1$, the fraction of strong spins $c = N_1/N$, and the temperature T. We use J_1, J_1/k_B and k_B for the units of the energy, temperature, and the entropy, respectively, where k_B is the Boltzmann constant. All the results are obtained in the thermodynamic limit.

3.3 Free energy calculation

We calculate the free energy of the model using the standard replica method. In the method, the free energy of the original model is obtained by taking the limit $n \to 0$ of the free energy of n replicas. The procedure of this calculation for the one-component PSM is well documented in Ref. [41, 43]. Following the same procedure, we write down the free energy of the two-component PSM as

$$-F/T = \lim_{n\to 0} \frac{1}{2n} \max G_n(Q, P) \tag{3.3}$$

with

$$\begin{aligned} G_n = \sum_{ab} \frac{1}{2T^2} \Big[&(cQ_{ab})^3 + 3J^2(cQ_{ab})^2((1-c)P_{ab}) + 3J^2(cQ_{ab})((1-c)P_{ab})^2 \\ &+ J^2((1-c)P_{ab})^3 \Big] + c \log\det Q + (1-c)\log\det P + n(1+\log 2\pi), \end{aligned} \tag{3.4}$$

where Q and P denote the overlap matrices for the component 1 and 2, each component of which is defined by $Q_{ab} = \frac{1}{N_1}\sum_i \sigma_{1,i}^{(a)}\sigma_{1,i}^{(b)}$ and $P_{ab} = \frac{1}{N_2}\sum_i \sigma_{2,i}^{(a)}\sigma_{2,i}^{(b)}$. $\max G_n(Q, P)$ means that the function G_n is maximized with respect to the matrices Q and P.

3.3.1 1RSB ansatz

In the case of the one-component PSM, it is known that the 1RSB ansatz gives the correct solution. The 1RSB ansatz assumes that the overlap matrices have a one-step hierarchical structure. In our model, this ansatz reads explicitly

$$Q_{ab} = (1-q_1)\delta_{ab} + (q_1 - q_0)\epsilon_{ab}^{m_1} + q_0, \tag{3.5}$$

$$P_{ab} = (1-p_1)\delta_{ab} + (p_1 - p_0)\epsilon_{ab}^{m_1} + p_0, \tag{3.6}$$

where δ_{ab} is the Kronecker delta and

$$\epsilon_{ab}^{m_1} = \begin{cases} 1 & if\ a \text{ and } b \text{ are in a diagnal block of } m_1 \times m_1 \\ 0 & \text{otherwise.} \end{cases} \tag{3.7}$$

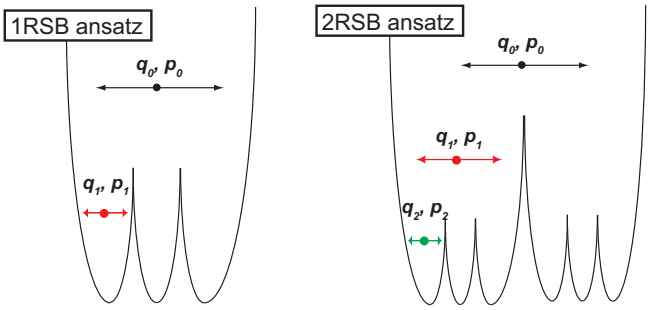

Figure 3.1: Sketch of the free energy landscapes corresponding to the 1RSB solution (left) and the 2RSB solution (right). There is the intermediate level of the hierarchy of states in the 2RSB solution.

Here, q_1 and p_1 are called the self overlaps, which are the overlaps within the same glassy states, and q_0 and p_0 are the overlaps between different glassy states (Figure 3.1 left). We can assume $q_0 = p_0 = 0$ that is valid for the PSM without external fields. Substituting equations (3.5) and (3.6) into equation (3.4), and taking the limit $n \to 0$ in equation (3.3), we obtain

$$-F/T = \frac{1}{2}(1 + \log 2\pi) + x_1 + x_2 + x_3 + x_4 + \min_{m_1,q_1,p_1} G_{1RSB} \tag{3.8}$$

with

$$\begin{aligned} G_{1RSB} = (m_1 - 1)[x_1 q_1^3 + x_2 q_1^2 p_1 + x_3 q_1 p_1^2 + x_4 p_1^3] \\ + \frac{c}{2}\left[\log(1 - q_1) + \frac{1}{m_1}\log\frac{1 + (m_1 - 1)q_1}{1 - q_1}\right] \\ + \frac{1 - c}{2}\left[\log(1 - p_1) + \frac{1}{m_1}\log\frac{1 + (m_1 - 1)p_1}{1 - p_1}\right], \end{aligned} \tag{3.9}$$

where $x_1 = c^3/4T^2$, $x_2 = 3c^2(1 - c)J^2/4T^2$, $x_3 = 3c(1 - c)^2J^2/4T^2$, and $x_4 = (1 - c)^3J^2/4T^2$. The breaking parameter m_1 should be limited to $0 \leq m_1 \leq 1$ in the limit $n \to 0$. When $m_1 = 1$, this 1RSB free energy reduces to that of the paramagnetic state. When G_{1RSB} is extremized with respect to q_1, p_1, and m_1, the 1RSB solution of the model is obtained. The 1RSB dynamical transition is defined as the transition where the overlaps q_1 and p_1 change discontinuously, and the 1RSB thermodynamic transition is defined as the transition where the 1RSB solution with $m_1 \neq 1$ becomes stable.

3.3.2 2RSB ansatz

Our model is the two component PSM with the two distinct energy scales J_1 and J_2, which make the thermodynamic phase diagram more complex. Especially there is no guarantee that the 1RSB ansatz gives the stable solution. Therefore, we have to allow the two-step hierarchical structure of the overlap matrices:

$$Q_{ab} = (1 - q_2)\delta_{ab} + (q_2 - q_1)\epsilon_{ab}^{m_2} + (q_1 - q_0)\epsilon_{ab}^{m_1} + q_0, \tag{3.10}$$
$$P_{ab} = (1 - p_2)\delta_{ab} + (p_2 - p_1)\epsilon_{ab}^{m_2} + (p_1 - p_0)\epsilon_{ab}^{m_1} + p_0, \tag{3.11}$$

which are called the 2RSB ansatz. This ansatz corresponds to the two-step hierarchical structure of the free energy landscape as depicted schematically in Figure 3.1 right. Here, q_2 and p_2 are the self overlaps, q_1 and p_1 are the overlaps between the different glassy states in the same group in the intermediate level of the hierarchy, and q_0 and p_0 are the overlaps between the different glassy states in the different groups. Substituting equations (3.10) and (3.11) into equation (3.4) and taking the limit $n \to 0$ in equation (3.3), we obtain

$$-F/T = \frac{1}{2}(1 + \log 2\pi) + x_1 + x_2 + x_3 + x_4 + \min_{m_1,m_2,q_1,q_2,p_1,p_2} G_{2RSB} \tag{3.12}$$

with

$$\begin{aligned} G_{2RSB} = {} & (m_2 - 1)[x_1 q_2^3 + x_2 q_2^2 p_2 + x_3 q_2 p_2^2 + x_4 p_2^3] \\ & + (m_1 - m_2)[x_1 q_1^3 + x_2 q_1^2 p_1 + x_3 q_1 p_1^2 + x_4 p_1^3] \\ & + \frac{c}{2}\Big[\log(1 - q_2) + \frac{1}{m_1}\log\frac{1 + (m_2 - 1)q_2 + (m_1 - m_2)q_1}{1 + (m_2 - 1)q_2 - m_2 q_1} \\ & + \frac{1}{m_2}\log\frac{1 + (m_2 - 1)q_2 - m_2 q_1}{1 - q_2}\Big] \\ & + \frac{1 - c}{2}\Big[\log(1 - p_2) + \frac{1}{m_1}\log\frac{1 + (m_2 - 1)p_2 + (m_1 - m_2)p_1}{1 + (m_2 - 1)p_2 - m_2 p_1} \\ & + \frac{1}{m_2}\log\frac{1 + (m_2 - 1)p_2 - m_2 p_1}{1 - p_2}\Big]. \end{aligned} \tag{3.13}$$

The breaking parameters m_1 and m_2 should be limited to $0 \leq m_1 < m_2 \leq 1$. When $m_2 = 1$, the 2RSB free energy G_{2RSB}, equation (3.13), reduces to

the 1RSB free energy G_{1RSB}, equation (3.9). By minimizing G_{2RSB} in equation (3.13) with respect to the order parameters q_1, p_1, q_2, p_2, m_1 and m_2, the free energy and the order parameters of the original system is obtained within the 2RSB ansatz. The 2RSB dynamical transition is defined as the transition where the overlaps q_2 and p_2 change discontinuously, and the 2RSB thermodynamic transition is defined as the transition where the 2RSB solution with $m_2 \neq 1$ becomes stable [1].

3.3.3 Numerical minimization of G_{2RSB}

We focus on the minimization of G_{2RSB}. We do not need to analyze G_{1RSB} separately, because G_{1RSB} is included in G_{2RSB} as discussed above. We employ the following numerical method to minimize G_{2RSB}. For a given c, we first focus on a low enough temperature (in practice, we set $T = J/3$) and minimize G_{2RSB} by the steepest descent method. We take a special care in this procedure because the calculation easily gets stuck in locally stable solutions. In order to avoid this unwanted effect, we first slice the (m_1, m_2) space to 50 grid points and minimize G_{2RSB} with respect to q_1, p_1, q_2 and p_2 at each grid point. We seek for the set of (m_1, m_2) which minimizes G_{2RSB}. Using this (m_1, m_2) as an initial guess, we perform the full steepest descent optimization of all the order parameters. After obtaining the optimized solution at the lowest temperature, we gradually increase the temperature and employ the steepest descent method to minimize G_{2RSB} at each temperature, using the optimal values of the order parameters at the lower temperature as an initial guess.

3.4 Phase diagrams and thermodynamic quantities

In this section, we show the phase diagrams and the thermodynamic quantities of the two-component PSM obtained by the minimization of G_{2RSB}. We find that the model has a variety of glass phases including the "single" and the "double" glasses when J is very different from 1.

[1] We did not explore the possibilities of RSB of the higher order than 2RSB. Note that the 2RSB is guaranteed to be sufficient at least in the limit $J \to 0$ because this limit corresponds to the randomly pinned PSM where the solution corresponding to the 2RSB is verified to be stable [80].

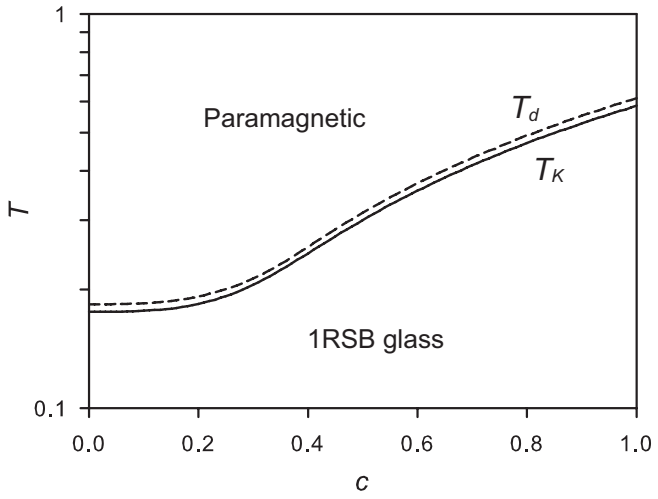

Figure 3.2: The phase diagram of the two-component PSM at $J = 0.3$. T_d (dashed line) is the 1RSB dynamical transition temperatures; T_K (solid line) is the 1RSB thermodynamic transition temperatures. There is only one glass phase characterized by the 1RSB solution at $J = 0.3$.

3.4.1 Order parameters and phase diagrams

$J = 0.3$.

We start with $J = 0.3$, which is not very different from 1. We show the phase diagram in Figure 3.2. There are only the paramagnetic phase and the 1RSB glass phase. The two phases are separated by the 1RSB thermodynamic transition line $T_K(c)$. The 1RSB dynamical transition line $T_d(c)$ is located at slightly higher temperatures. Note that $T_d(c)$ and $T_K(c)$ for $c = 1$ match with the results of the one-component PSM of the strong spins. They are $T_d(c = 1) = 0.612$ and $T_K(c = 1) = 0.586$. $T_d(c)$ and $T_K(c)$ for $c = 0$ are identical to those for $c = 1$ aside from the obvious factor of J, which defines the unit of the energy, i.e., $T_d(c = 0) = 0.612J = 0.184$ and $T_K(c = 0) = 0.586J = 0.176$. The transition lines smoothly connect these two limiting cases.

In order to gain more insights, in Figure 3.3, we plot the temperature dependence of the optimized overlaps q_1 and p_1 and the breaking parameter m_1 at two representative values of $c = 0.2$ and 0.9. At $c = 0.2$ (Figure 3.3 left), as temperature is decreased, the overlaps q_1 and p_1 jump from zero while the breaking parameter remains constant $m_1 = 1$ at the 1RSB dynamical

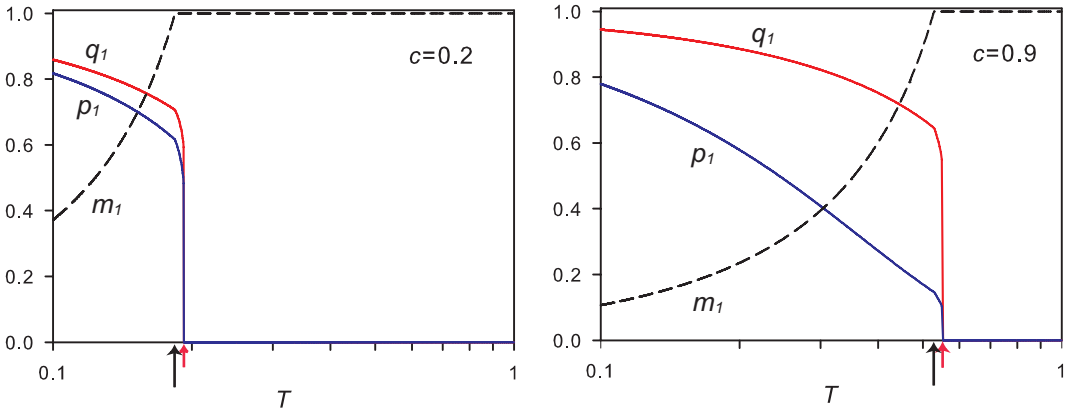

Figure 3.3: Temperature dependence of the overlaps q_1 and p_1 and the breaking parameter m_1 at $c = 0.2$ (left) and 0.9 (right) at $J = 0.3$. The short red and long black arrows indicate the 1RSB dynamical and thermodynamic transition temperatures T_d and T_K, respectively.

transition temperature T_d. m_1 suddenly starts decreasing from 1 at the 1RSB thermodynamic transition temperature T_K. The 1RSB dynamical and thermodynamic transition temperatures ($T_d(c = 0.2) = 0.192$ and $T_K(c = 0.2) = 0.184$) are close to those of the one-component PSM of weak spins ($T_d(c = 0) = 0.184$ and $T_K(c = 0) = 0.176$), indicating that the 1RSB transition at $c = 0.2$ is driven mainly by the freezing of the weak spins. Note that both the values of q_1 and p_1 just below the transition temperatures are larger than 0.5 and are close to each other, which can be interpreted that both the strong and weak spins are frozen equally strongly at this transition.

Behaviors at $c = 0.9$ (Figure 3.3 right) are qualitatively similar to those at $c = 0.2$. The only differences are that (i) the 1RSB dynamical and thermodynamic transition temperatures ($T_d(c = 0.9) = 0.552$ and $T_K(c = 0.9) = 0.528$) are close to those of the one-component PSM of the *strong* spins ($T_d(c = 1) = 0.612$ and $T_K(c = 1) = 0.586$) and that (ii) the value of q_1 is larger than 0.5 while the value of p_1 is much smaller just below the transition temperatures. These results can be interpreted that the 1RSB transition at $c = 0.9$ is driven mainly by the freezing of the strong spins, and the weak spins are not strongly frozen at this transition. However we emphasize that this difference is only quantitative and the overlaps of the weak and strong spins vary continuously as c changes. Namely there is no clear signature of the decoupling of the glass transitions of the weak and strong spins.

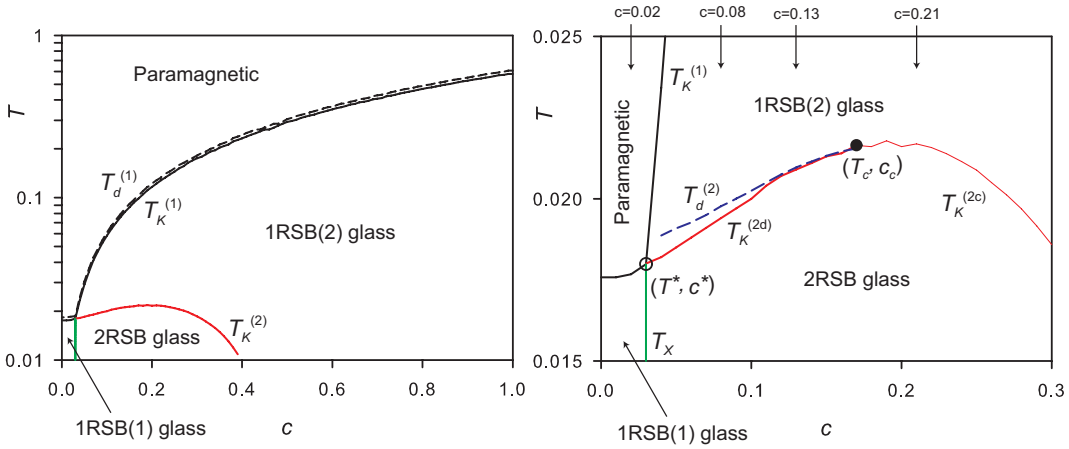

Figure 3.4: The phase diagram at $J = 0.03$. (left) Overall view. There are the paramagnetic phase and the three glass phases, the 1RSB(1), the 1RSB(2), and the 2RSB. $T_d^{(1)}$ and $T_K^{(1)}$ are the 1RSB dynamical and thermodynamic transition temperatures, respectively. $T_K^{(2)}$ is the 2RSB thermodynamic transition temperature. (right) Zoom on the the 2RSB glass region. $T_K^{(2)}$ is composed of the discontinuous and continuous 2RSB transition temperatures, $T_K^{(2d)}$ and $T_K^{(2c)}$. $T_d^{(2)}$ is the 2RSB dynamical transition temperature, which terminates at the critical point $(T_c, c_c) \approx (0.022, 0.17)$. T_X is the phase boundary between the 1RSB(1) and the 2RSB glass phases. The three thermodynamic transition lines, $T_K^{(1)}$, $T_K^{(2d)}$, and T_X, meet at $(T^\star, c^\star) \approx (0.018, 0.03)$. The four downwards arrows indicate the four representative values of c, for which the temperature evolutions of the overlaps and the thermodynamic quantities are presented in Figures 3.5 and 3.7.

$J = 0.03$.

Next we focus on $J = 0.03$, which is much smaller than 1. In Figure 3.4 left, we show the phase diagram, which is qualitatively different from that at $J = 0.3$. One finds that there are three glass phases. We refer to them as the 1RSB(1), the 1RSB(2), and the 2RSB glass phases. The paramagnetic phase is separated from the 1RSB(1) and the 1RSB(2) glass phases by the 1RSB thermodynamic transition line $T_K^{(1)}(c)$. The associated 1RSB dynamical transition line $T_d^{(1)}(c)$ is located at slightly above $T_K^{(1)}(c)$. The 2RSB glass phase is located below the 1RSB(2) glass phase. The 1RSB(2) and the

2RSB glass phases are separated by the 2RSB thermodynamic transition line $T_K^{(2)}(c)$. To present the details of the 2RSB glass phase region, we show the zoom in Figure 3.4 right. The 2RSB thermodynamic transition line $T_K^{(2)}(c)$ is composed of two parts: $T_K^{(2d)}(c)$ at lower fraction of strong spins and $T_K^{(2c)}(c)$ at higher fraction of strong spins, depending on the discontinuous and continuous nature of the transition across this temperature. The 2RSB dynamical transition line $T_d^{(2)}(c)$ is located at slightly above $T_K^{(2d)}(c)$ and it terminates at the critical point $(T_c, c_c) \approx (0.022, 0.17)$, at which the three transition lines $T_d^{(2)}(c)$, $T_K^{(2d)}(c)$ and $T_K^{(2c)}(c)$ meet. The thermodynamic transition line which separates the 1RSB(1) glass from the 2RSB glass is denoted as $T_X(c)$. The three thermodynamic transition lines, $T_K^{(1)}(c)$, $T_K^{(2d)}(c)$ and $T_X(c)$, meet at the point $(T^\star, c^\star) \approx (0.018, 0.03)$, which is the meeting point of all the four phases. As c increases, the 1RSB thermodynamic transition line $T_K^{(1)}(c)$ sharply bends upward at this point and the transition into the 1RSB(1) glass becomes the transition into the 1RSB(2) glass.

In order to understand the nature of these phases, we plot the temperature dependence of the overlaps and the breaking parameters at four representative values of $c = 0.02$, 0.08, 0.13, and 0.21, in Figure 3.5. These values of c are indicated as arrows in the phase diagram, see Figure 3.4 right. We first focus on $c = 0.02$ (Figure 3.5 upper left). When the temperature is decreased from above, q_1 and p_1 change discontinuously from zero at the 1RSB dynamical transition temperature $T_d^{(1)}$. While m_2 remains to be unity, m_1 suddenly starts decreasing from 1 at $T_K^{(1)}$, where the 1RSB thermodynamic transition from the paramagnetic phase to the 1RSB(1) glass phase takes place. Note that the 1RSB dynamical and thermodynamic transition temperatures ($T_d^{(1)}(c = 0.02) = 0.0185$ and $T_K^{(1)}(c = 0.02) = 0.0177$) are close to those of the one-component PSM of the weak spins ($T_d^{(1)}(c = 0) = 0.0184$ and $T_K^{(1)}(c = 0) = 0.0176$), which indicates that the transition into the 1RSB(1) glass phase is driven mainly by the freezing of the weak spins. Both the values of q_1 and p_1 are larger than 0.5 and are close to each other below $T_K^{(1)}$, which can be interpreted that both the strong and weak spins are frozen equally strongly in the 1RSB(1) glass phase.

The upper right panel of Figure 3.5 shows the results at $c = 0.08$, where there are the 1RSB transition from the paramagnetic to the 1RSB(2) glass phase, and the 2RSB transition from the 1RSB(2) to the 2RSB glass phase. The 1RSB dynamical and thermodynamic transitions at $T_d^{(1)}$ and $T_K^{(1)}$ are

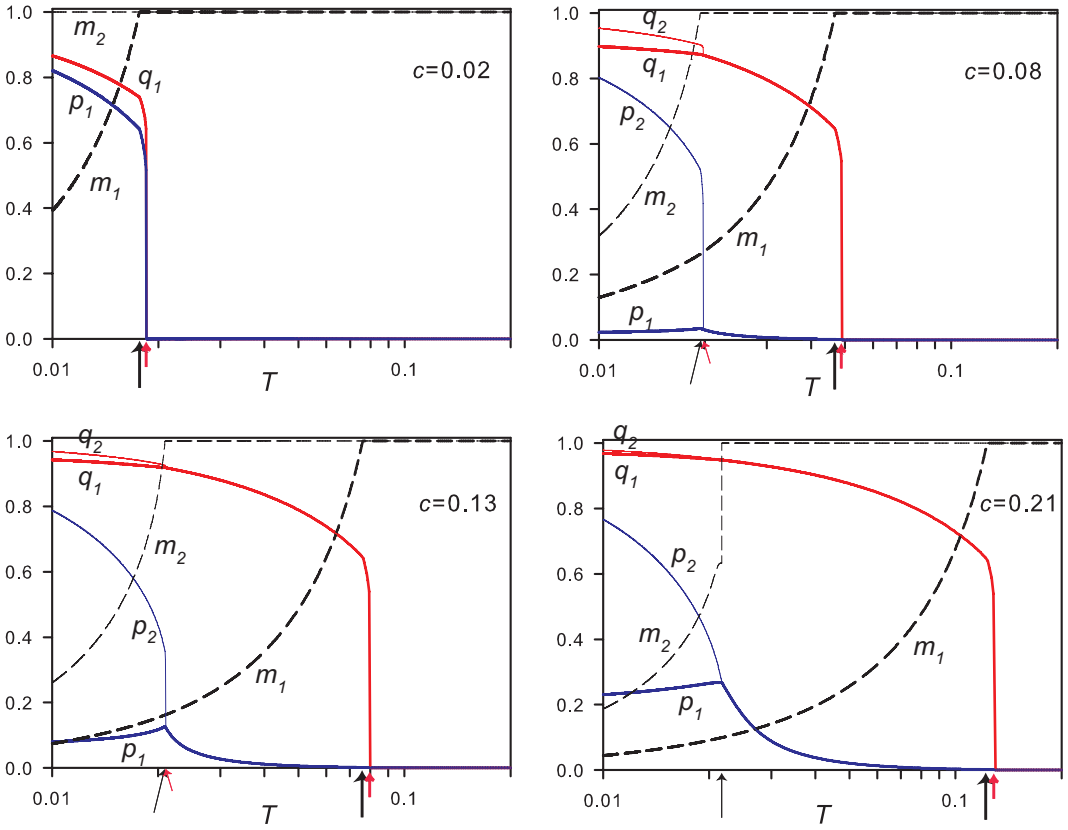

Figure 3.5: Temperature dependence of the overlaps, q_1, p_1, q_2, and p_2, and the breaking parameters, m_1, and m_2, at $c = 0.02$ (upper left), 0.08 (upper right), 0.13 (lower left) and 0.21 (lower right) at $J = 0.03$. The bold short red and long black arrows indicate the 1RSB dynamical and thermodynamic transition temperatures T_d and T_K, respectively; the thin short red and long black arrows indicate the 2RSB dynamical and thermodynamic transition temperatures $T_d^{(2)}$ and $T_K^{(2d)}$ ($T_K^{(2c)}$ for $c = 0.21$), respectively,

qualitatively the same as those for $c = 0.02$. The only difference is that the value of q_1 is larger than 0.5 while p_1 is very close to zero. This result can be interpreted that the strong spins are frozen while the weak spins are *not* frozen in the 1RSB(2) glass phase. As we decrease temperature further, the 2RSB transition takes place. First at $T_d^{(2)}$, the overlaps q_2 and p_2 change discontinuously while the breaking parameter remains constant $m_2 = 1$. At $T_K^{(2d)}$, m_2 suddenly starts decreasing from 1, where the 2RSB thermodynamic transition takes place. Note that p_2 is larger than 0.5 just below $T_K^{(2d)}$, which can be interpreted that the weak spins are also frozen in the 2RSB glass phase.

Behaviors at $c = 0.13$ (Figure 3.5 lower left) are qualitatively similar to those at $c = 0.08$. The only difference is that the discontinuities of q_2 and p_2 at the 2RSB dynamical transition are smaller than those for $c = 0.08$. As c increases, the discontinuities at the 2RSB dynamical transition become smaller, and eventually the jump of q_2 and p_2 disappear at $c = 0.17$. The lower right panel of Figure 3.5 shows the results at $c = 0.21$. The overlaps q_2 and p_2 change from q_1 and p_1 continuously at $T_K^{(2c)}$, where the continuous 2RSB thermodynamic transition takes place. Interestingly, the change of the breaking parameter m_2 at $T_K^{(2c)}$ is not continuous as in the case at $T_K^{(2d)}$ but discontinuous.

In summary, the 1RSB(2) glass corresponds to the "single" glass where only the strong spins are frozen, and the 1RSB(1) and the 2RSB glasses correspond to the "double" glass where both the weak and strong spins are frozen simultaneously. We emphasize that there is a clear difference between these two "double" glasses, the 1RSB(1) and the 2RSB. The transition into the 1RSB(1) glass phase is the simultaneous arrest of the weak and the strong spins. This transition is mainly driven by the freezing of the weak spins. On the other hand, the transition into the 2RSB glass phase is the arrest of the weak spins in the presence of the frozen strong spins which already undergoes the glass transition at much higher temperature. The difference becomes clearer when one considers the free energy landscape of these phases. In the 1RSB(1) glass phase, the landscape can be characterized by the one-step hierarchical structure (Figure 3.1 left). Only the self overlap q_1 and p_1 have large values, and q_0 and p_0 are zero. This means that the different glassy states have completely different configurations of spins. On the other hand in the 2RSB glass phase, the landscape has the two-step hierarchical structure (Figure 3.1 right). Not only the self overlaps q_2 and p_2, but also

the overlap q_1 have large values. This means that several glassy states in the same group of the intermediate level of the hierarchy share almost the same configuration of the strong spins. In other words, the phase space is divided into a multi-valley structure corresponding to configurations of the strong spins and each of the valley is divided into a subgroups of multi-valley structure corresponding to configurations of the weak spins. Note that the 1RSB(1) and the 2RSB glasses are separated by the glass-glass transition T_X as shown in Figure 3.4. As one crosses T_X, the overlaps discontinuously change (not shown).

Finally we obtain a semi-analytical expression for the continuous 2RSB transition temperature $T_K^{(2c)}$. This is possible because $q_2 - q_1$ and $p_2 - p_1$ are small just below $T_K^{(2c)}$ and thus the 2RSB solution can be expressed by the perturbation around the 1RSB solution (see Appendix for details). In Figure A.1, we compare $T_K^{(2c)}$ calculated by the perturbation theory with those calculated by the minimization of G_{2RSB}. The two results are almost identical, confirming that our numerical minimization of G_{2RSB} is reliable.

The decoupling of the glass transitions of the weak and the strong spins.

We showed that there is only one glass phase at $J = 0.3$, whereas at $J = 0.03$ the decoupling of the glass transitions of the weak and the strong spins takes place and, as a result, the three glass phases appear. In this subsection, we estimate the value of $J = J^\star$ at which this decoupling sets in.

First we evaluate the phase diagram at various J in the range of $0.03 < J < 0.3$ by the minimization of G_{2RSB}. We find that the three glass phases exist at $J \leq 0.1$ while only one glass phase exists at $J \geq 0.2$. This means $0.1 < J^\star < 0.2$. However we can not estimate $J^\star$ more accurately by this procedure. Our numerical minimization becomes unstable at $0.1 < J < 0.2$ because the free energy differences between G_{1RSB} and G_{2RSB} become small.

In the course of the evaluations of the phase diagrams described above, we find that whenever there exist the three glass phases, there also exists the glass-glass transition point ($T^\star$, $c^\star$) from the 1RSB(1) to the 1RSB(2) glass phase on the line $T_K^{(1)}(c)$, see Figure 3.4. Here, we estimate $J^\star$ assuming that $J^\star$ is identical to the value of J just below which the glass-glass transition point appears on the line $T_K^{(1)}(c)$. We evaluate the overlaps along the line $T_K^{(1)}(c)$, and seek for the discontinuous jump of the overlaps as a function of

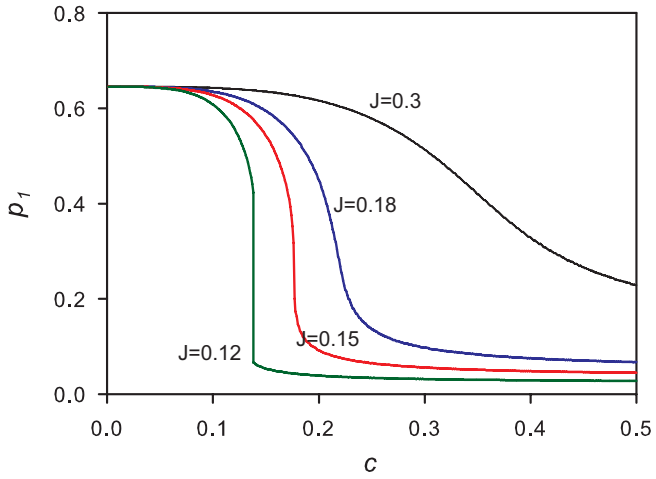

Figure 3.6: The overlap of weak spins p_1 against c on the 1RSB thermodynamic transition line $T_K^{(1)}(c)$ at various values of J. The glass-glass transition point appears at $J \approx 0.15$.

c, which is the sign of the glass-glass transition. This analysis is numerically easier than the full evaluation of the phase diagram because it requires the numerical minimization only of G_{1RSB}. In Figure 3.6, we show the c dependence of the overlap of weak spins p_1 on the line $T_K^{(1)}(c)$, at several values of J. At $J = 0.3$, p_1 decreases smoothly with c and there is no glass-glass transition point. The decrease of p_1 becomes sharper with decreasing J, and becomes discontinuous just below $J \approx 0.15$. From this calculation, we estimate $J^\star \approx 0.15$.

3.4.2 Thermodynamic quantities

In this subsection, we discuss the nature of the various glass phases of the model in terms of the thermodynamic quantities.

Figure 3.7 shows the temperature dependence of the entropy $S = -\partial F/\partial T$ and the heat capacity $C = -T\partial^2 F/\partial T^2$ at $J = 0.03$ at the same values of c in Figure 3.5. These quantities are evaluated by numerical differentiation of the free energy obtained by the minimization of G_{2RSB}. At $c = 0.02$ (Figure 3.7 upper left), the entropy curve bends and the heat capacity jumps discontinuously at the 1RSB thermodynamic transition temperature $T_K^{(1)}$. This is the typical behavior of the 1RSB glass transition. On the other hand

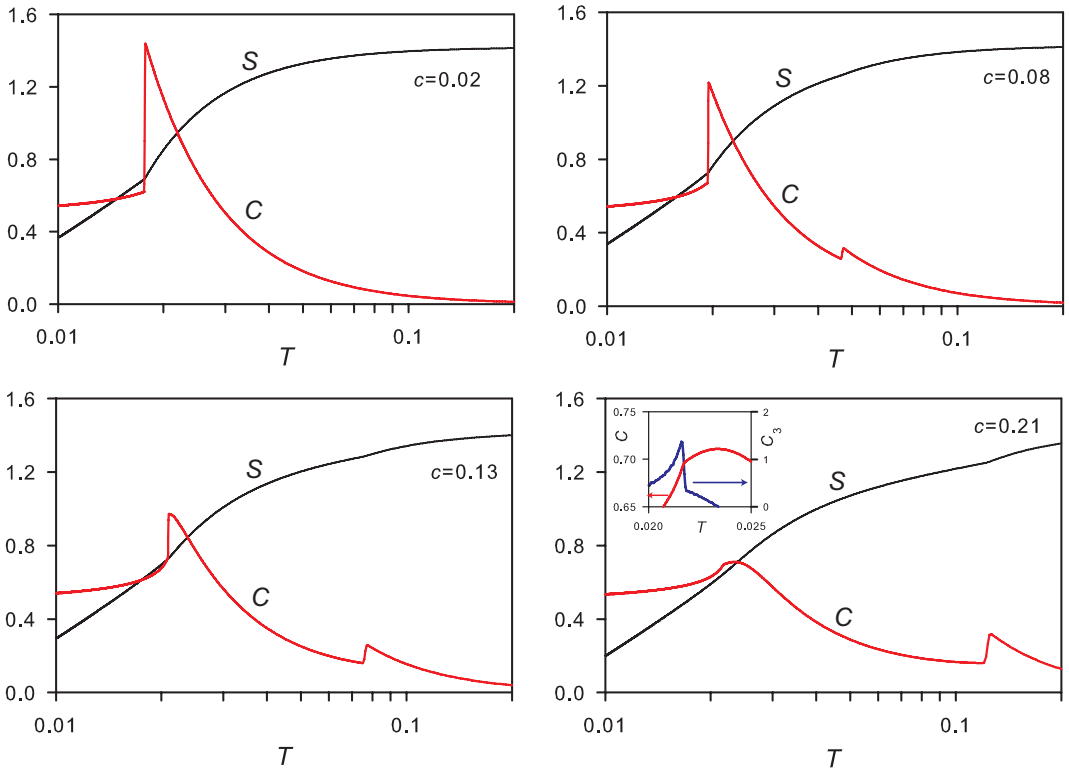

Figure 3.7: Temperature dependence of the entropy S and the heat capacity C at $c = 0.02$ (upper left), 0.08 (upper right), 0.13 (lower left) and 0.21 (lower right) at $J = 0.3$. Inset of the lower right panel shows the heat capacity C and the third order derivative of the free energy C_3 at around the continuous 2RSB thermodynamic transition temperature $T_K^{(2c)}$.

at $c = 0.08$ (Figure 3.7 upper right), the entropy curve bends and the heat capacity jumps twice at the 1RSB and the 2RSB thermodynamic transition temperatures, $T_K^{(1)}$ and $T_K^{(2d)}$. As can be seen from the results at $c = 0.13$ (Figure 3.7 lower left) and 0.21 (Figure 3.7 lower right), the heat capacity jump at $T_K^{(2d)}$ becomes weaker with increasing c and eventually disappears when the 2RSB transition becomes continuous. In order to characterize the thermodynamics of the continuous 2RSB thermodynamic transition, we plot the third order derivative of the free energy $C_3 = T^2\partial^3 F/\partial T^3$ in the inset of Figure 3.7 lower right. One finds that this quantity shows the discontinuous jump at the continuous 2RSB transition temperature $T_K^{(2c)}$. Thus the continuous 2RSB transition is the third-order thermodynamic transition in nature. Note that the similar behavior has been observed for the continuous 1RSB transition [41].

3.5 Discussion

We found that the two-component PSM has three glass phases at $J \leq 0.15$: the 1RSB(1) glass where both the strong and weak spins are frozen, the 1RSB(2) glass where only the strong spins are frozen, and the 2RSB glass where both the strong and weak spins are frozen and the free energy landscape has the two-step hierarchical structure. In this section, we discuss possible connections and implications of these results to other systems.

3.5.1 Connection to the randamly pinned PSM

In the randomly pinned PSM, a fraction of spins are pinned and the dynamics and thermodynamics of remaining mobile spins are considered. This model has recently attracted attention partly, because it enables us to probe the true thermodynamic glass transition without waiting for the system to equilibrate, which otherwise takes astronomically long time [80–82]. Interestingly, the 2RSB dynamical and thermodynamic transition lines (see Figure 3.4 right) are analogous to the glass transition lines of the randomly pinned glass [80]. In both cases, the overlap discontinuously jumps at the dynamical transition lines when the density of the pinned spins (for the randomly pinned PSM) or the strong spins (for the two-component PSM) is small. But as the densities increase the discontinuities are weakened and eventually the transitions become continuous at which the dynamical transition lines ter-

minate. The similarity between these two models is natural because, in the two-component PSM, the strong spins frozen at higher temperature behaves as the "randomly pinned spins" in the sea of the mobile weak spins at lower temperature. Indeed we can establish the precise relation between these two models. To this end, we focus on the behaviors of weak spins in the limit of $J \to 0$ while keeping T/J constant. In this limit, the overlaps of strong spins become $q_2 = 1$, $q_1 = 1$ and the breaking parameter $m_1 = 0$. Plugging these limiting values into G_{2RSB}, equation (3.13), the relevant part for the weak spins becomes

$$G_{2RSB} \sim (m_2 - 1)[x_1 + x_2 p_2 + x_3 p_2^2 + x_4 p_2^3] - m_2[x_1 + x_2 p_1 + x_3 p_1^2 + x_4 p_1^3] + \frac{1-c}{2}\Big[\log(1-p_2) + \frac{p_1}{1 + (m_2 - 1)p_2 - m_2 p_1} + \frac{1}{m_2}\log\frac{1 + (m_2 - 1)p_2 - m_2 p_1}{1 - p_2}\Big]. \tag{3.14}$$

This free energy is essentially equivalent to the one of the randomly pinned PSM [2]. Thus the phase diagram of the two-component PSM converges to that of the randomly pinned PSM in this limit.

3.5.2 Connection to the MCT of binary mixtures

We next discuss the implications of the two-component PSM for binary mixtures of large and small particles with disparate size ratio. The MCT was recently used to analyze the decoupling of the glass transitions of large and small particles in this model and predicted the existence of four distinct glass phases [71]: (i) The "partially frozen cageing" glass in which only the large particles are arrested due to the cageing effect amongst the large particles. In this phase, the small particles are left mobile and do not qualitatively affect the dynamics of large particles. (ii) The "partially frozen depletion-driven" glass in which only the large particles are arrested by a short-ranged but strong attractive interaction induced by the depletion effect caused by small particles [**?**, 83]. In both the phases (i) and (ii), only the large particles undergo the glass transition and the small particles play a role as the background solvent. The phase (i) is often called the repulsive glass and (ii) is the attractive glass [84–87]. (iii) The "fully frozen" glass in which both

[2] Equation (3.14) becomes equivalent to equation (16) in Ref. [80], after dividing equation (16) by n, taking carefully $n \to 0$ limit and replacing p_2, p_1 and m_1 with q_1, q_0 and m, respectively.

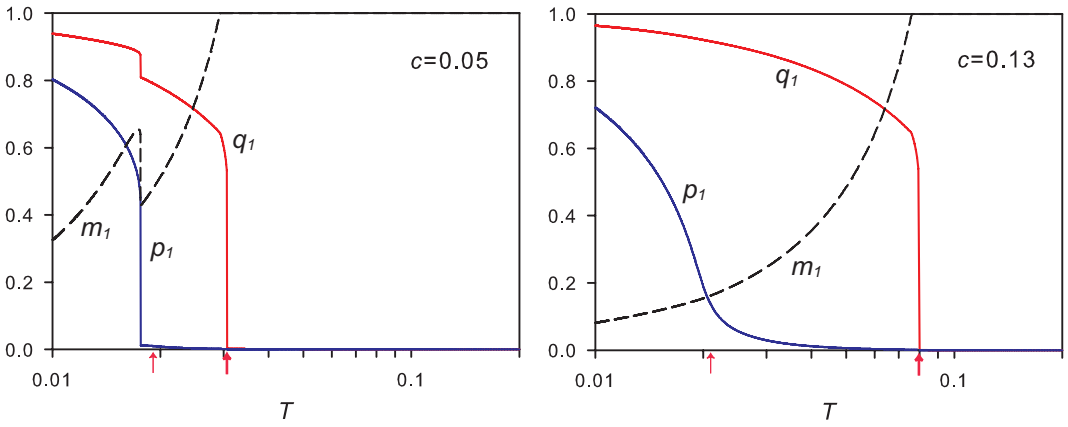

Figure 3.8: Temperature dependence of the overlaps q_1 and p_1 and the breaking parameter m_1 at $c = 0.05$ (left) and 0.13 (right) in the 1RSB solution at $J = 0.03$. The bold and thin red arrows indicate the 1RSB and the 2RSB dynamical transition temperatures, $T_d^{(1)}$ and $T_d^{(2)}$, respectively. The 1RSB solution captures a trace of the 2RSB dynamical transition at $c = 0.05$, while does not at $c = 0.13$.

the large and small particles are arrested simultaneously. Both the large and small particles equally contribute to the formation of the frozen states. (iv) The "torronchino" glass which is a subset of the "fully frozen" glass. In this phase, however, the number of the small particles is much larger than that of the large particles and the freezing is driven mainly by the small particles. By comparing the glass phases in our model with those of the MCT, one finds that the "partially frozen cageing" glass corresponds to the 1RSB(2) glass, the "fully frozen" to the 2RSB, and the "torronchino" to the 1RSB(1). Because there is no depletion effect in the present model, there is no phase corresponding to the "partially frozen depletion-driven" glass. At this stage however, one should realize a subtle but important difference between the descriptions of the MCT and the replica theory for these phases. Specifically, we revealed that the two-step replica symmetry breaking is needed to describe the 2RSB glass or the "fully frozen" glass. However the MCT is believed to be a theory of the 1RSB dynamical transition [2, 4], therefore it cannot intrinsically describe this phase.

In order to consider the validity of the prediction of the MCT for the 2RSB glass phase, it is useful to see how the 1RSB solution behaves in the

2RSB glass phase [3]. In Figure 3.8, we plot the temperature dependence of the overlaps of the 1RSB solution at $J = 0.03$. At $c = 0.05$ (Figure 3.8 left), p_1 and q_1 jump not only at the 1RSB dynamical transition temperature $T_d^{(1)}$ but also at around the 2RSB dynamical transition temperature $T_d^{(2)}$. This means that though the 1RSB solution is incorrect in the 2RSB glass region, it captures a signature of the transition into the 2RSB glass phase to a certain extent. At $c > 0.08$, however, we do not find any signature of the 2RSB dynamical transition in the 1RSB solution. Indeed at $c = 0.13$ (Figure 3.8 right), q_1 and p_1 increase only smoothly with decreasing temperature in the glass phase, while the 2RSB solution predicts the discontinuous 2RSB dynamical transition at $T_d^{(2)}$ (Figure 3.5 lower left). In summary, the 1RSB solution can not correctly describe the 2RSB glass phase although it can capture a trace of the 2RSB transition for a certain range of parameters. This suggests that the applicability of the MCT to describe the decoupling of the glass transitions in binary mixtures with disparate size ratio may be questioned.

3.6 Conclusions

In this work, we have introduced and studied a two-component version of the p-spin spherical model. The model is composed of strongly interacting spins (strong spins) and weakly interacting spins (weak spins), which mimic the glass forming binary mixtures of large and small particles with disparate size ratio. We have found that when the strengths of the interactions of the weak and strong spins are not widely separated, the model has only one glass phase. This glass phase is the frozen state of both the strong and weak spins and is described by the conventional 1RSB solution. On the other hand when the strengths of the interactions are well separated, the model exhibits the decoupling of the glass transitions of the weak and strong spins and, as a result, there appear the three distinct glass phases. We referred to them as the 1RSB(1), the 1RSB(2), and the 2RSB glass phases. The 1RSB(1) glass phase appears in the region where the number fraction of the strong spins is very small. This glass phase is the frozen state of both the strong and weak spins, although the transition into this phase is driven mainly by the freezing

[3]More precisely, the MCT solution corresponds to the 1RSB solution optimized with leaving $m_1 = 1$. We also performed this calculation and verified that the results discussed below are qualitatively unchanged.

of the weak spins. The 1RSB(2) glass phase appears in the region where the number fraction of the strong spins is large. In this glass phase, only the strong spins are frozen while the weak spins are left mobile. By cooling the 1RSB(2) glass further, the 2RSB glass phase is obtained, in which the weak spins are also frozen. The 2RSB glass phase is characterized by the two-step hierarchical structure of the free energy landscape. The 2RSB glass transition becomes ether discontinuous or continuous depending on the number fraction of the strong spins. The discontinuous 2RSB thermodynamic transition is accompanied with the jump of the second order derivative of the free energy, namely the heat capacity. On the other hand, for the continuous 2RSB thermodynamic transition, the heat capacity changes continuously while the third order derivative of the free energy jumps discontinuously. Based on the results, we have discussed the connection of the present model to the randomly pinned PSM. The phase diagram of the present model appears to be similar to that of the randomly pinned PSM. We have analytically showed that the free energy of the two-component PSM becomes exactly identical to that of the randomly pinned PSM in the small limit of the ratio between the strengths of the interactions of the weak and strong spins. We have also discussed the implications of the present results for the MCT for binary mixtures of large and small particles with disparate size ratio. We have found that the 1RSB solution can not correctly describe the 2RSB glass phase although it can capture a trace of the 2RSB transitions for a certain range of parameters, which may leave questionable the applicability of the MCT to describe the decoupling of the glass transitions in binary mixtures with disparate size ratio. Regarding this point, it is interesting to extend the replicated liquid state theory [21,22] to allow the 2RSB ansatz [88] to describe the decoupling of the glass transitions in binary mixtures with disparate size ratio. Study along this direction is under way [89].

Chapter 4

Replica liquid theory for binary mixtures of disparate size ratio

We develop a new formalism of the replica liquid theory which predicts the multiple glass phases of binary mixtures consists of large and small spherical spheres with disparate size ratio. This is possible by taking into account the two-step replica symmetry breaking, which is physically caused by the emergence of the two-step hierarchical energy landscape. We apply the theory to a harmonic potential fluid in the high dimensional limit and determine its phase diagram. We find that there exist three distinct glass phases when the size ratio between large and small particles is disparate; the normal glass phase where both components freeze simultaneously, the partially frozen phase where only large particles are frozen while small particles are mobile, the 2RSB glass phase where both components freeze simultaneously. The 2RSB glass phase, especially, is distinct from the normal glass phase in the structures of the energy landscapes.

4.1 Introduction

Introduction of size dispersity to particulate systems is a common strategy to obtain stable glass-forming systems. When the size ratio is close to unity, many of phenomenologies of the glass transition is not strongly affected by the size dispersity, except that the glass transition temperature and density depends on the size and component ratio. However when the size ratio is disparate, the decoupling phenomena is often observed, namely the dynamics

of a part of species decouples from that of the others and form a glass phase where only a part of species are frozen while the others remain mobile [32]. A wide variety of glassy materials including ionic glasses [31], metallic glasses [90], and polymeric glasses [91] exhibits this decoupling phenomena [32]. Among them, the simplest example is presumably the binary mixtures of large and small particles with disparate size ratio. In colloidal experiments [23,24,68] and simulations [25,26,69], it is established that this system has, at least, two glass phases depending on the component ratio: the "single" glass in which only the large particles are frozen and the "double" glass in which both types of particles are frozen. In the single glass, the small particles can diffuse through the gap among frozen large particles, in the way similar to the diffusion in a random media [92]. In the limit of the large size ratio, the single glass becomes the random version of the celebrated Lorentz gas model [93].

Currently, most of the theoretical approaches for the decoupling phenomena is based on the mode-coupling theory (MCT) of the glass transition [3, 33]. The naive extension of the MCT to the binary mixtures was shown to predict qualitatively the decoupling of the dynamics of small and large particles [70, 94] and the emergence of multiple glass phases [71]. However, it is not clear if the MCT and its further extensions finally give the full understanding of this phenomena because (1) the glass transition predicted by the MCT is known to be avoided due to the thermal activation, thus fictive in finite dimension [4, 95], (2) the MCT does not give a correct transition density even at infinite dimension (a mean-field limit) [74, 93], (3) even within the MCT framework, the choice of the slow variables has some arbitrariness and a different formulation gives a different result [96].

In this work, we propose a rather different approach, the *thermodynamic* description of the decoupling phenomena which are free from the above problems. Our theory is based on the replica liquid theory (RLT) [22,39,97]. For monodisperse particles, the RLT predicts two characteristic transition densities, φ_d and φ_K. When the density of the system is increased from the liquid state, the *dynamical transition* firstly takes place at φ_d, at which the phase space of the liquid state is divided into exponentially large number of metastable states or minima in the free-energy landscape. The logarithm of this number is the so-called configurational entropy Σ. The MCT is now believed to be a dynamical counter part of the mean-field description of the glass transition [35–37] which describes the slowing down of the dynamics at around φ_d. With increasing the density further, the configurational entropy

decreases and eventually becomes zero at φ_K where the *thermodynamic transition* takes place [36,37]. An important feature of the RLT is that the theory becomes exact in the limit of infinite dimension.

The conventional RLT was once extended to the binary mixtures [98–101]. However, it did not predict the decoupling phenomena irrespective of the size ratio. To understand the reason of this failure, we recently introduced and analyzed the spin-glass version of the binary mixtures [102]. We found that the assumption of the one-step replica symmetry breaking (1RSB) ansatz, which is commonly used in the RLT, is the origin of this failure and the decoupling phenomena can be described when we allow the two-step replica symmetry breaking (2RSB). In this work, we develop the RLT of the binary mixtures of particles taking into account the 2RSB. We find that the new RLT predicts the decoupling phenomena and explain the physical mechanism of it in terms of the energy landscape picture [103, 104]. Interestingly, the new theory does not only explain the single and double glass phases but it also predicts a new glass phase, which is characterized by the hierarchical free energy landscape. This prediction would stimulate further experimental and/or simulation investigations of binary mixtures.

4.2 Model

We investigate the binary mixture of Harmonic spheres [105]. The interaction potential of the model is

$$\begin{aligned} v_{\mu\nu}(r) &= \epsilon\phi(r/D_{\mu\nu}),\ \mu,\nu \in \{L,S\}, \\ \phi(r) &= (1-r)^2\theta(1-r), \end{aligned} \tag{4.1}$$

where we set $\epsilon = 1$ for simplicity. $v_{LL}(r)$, $v_{SS}(r)$ and $v_{LS}(r)$ denote the interaction potentials between large particles, small particles, and large and small particles, respectively. D_{LL} and D_{SS} mean the diameter of large and small particles, respectively. We use the additive potential *i.e.* $D_{LS} = (D_{LL} + D_{SS})/2$.

We study the model on the high dimensional limit. Here, we list several physical quantities in a convenient form on this limit. To obtain the non-trivial result on this limit, the potential should be rescaled as

$$\hat{\phi}(h) = d^2\phi\left(1 + \frac{h}{d}\right), \tag{4.2}$$

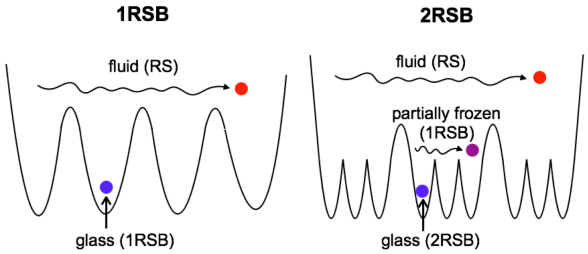

Figure 4.1: Schematic pictures of the free-energy landscape

with $h = d(r-1)$ [88,106]. The volume fractions of large and small particles are $\varphi_L = N_L v_d(D_{LL}/2)/V$ and $\varphi_S = N_S v_d(D_{SS}/2)/V$, respectively. $v_d(r)$ is the volume of the d-dimensional hyper-sphere, and N_L and N_S denote the number of large and small particles, respectively. We define the size ratio between large particles and small particles as $D_{LL}/D_{SS} = 1 + r/d$. The factor $1/d$ is necessary to keep the value of the relative volume finite, $v_d(D_{LL}/2)/v_d(D_{SS}/2) = (1 + r/d)^d \sim e^r$. Another relevant quantity is the fraction of small particles, $x = \varphi_S/(\varphi_L + \varphi_S)$.

4.3 1RSB Ansatz

A main idea of the RLT is to introduce the m copies of the original system (replicas) to evaluate the free energies of the liquid and glass phases. The overlap (similarity) between the configurations in different replicas plays the role of the order parameter of the glass transition. The conventional assumption in the RLT is the one-step replica symmetry breaking (1RSB) ansatz, which assumes that there are no overlap between the different metastable glassy states [22, 39, 97, 100]. The landscape considered in the 1RSB formalism is schematically shown in the left hand side of FIG. 4.1. The RLT with the 1RSB assumption is fully developed [22], especially on the high dimensional limit, and the application of it to the binary mixtures is straightforward [22,100]. We outline the calculation in Appendix B. The thermodynamic phase diagram predicted by this ansatz, however, only shows the RS phase, in which all particles are mobile, and the 1RSB phase, in which all particles are frozen, for all r (see Fig. B.1 in Appendix B). Thus, the 1RSB ansatz does not explain the decoupling phenomenon at least for the thermo-

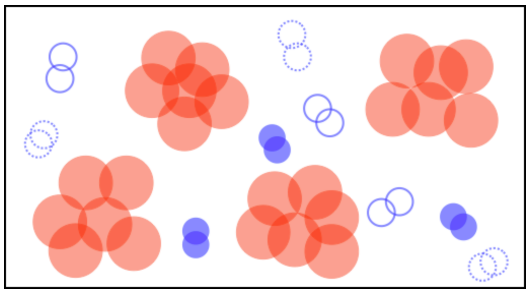

Figure 4.2: Schematic picture of the molecular system for $m = 6$ and $m_1 = 2$: The molecules composed of large particles are shown with the filled cycles. The $m/m_1 = 3$ kind of the molecules composed of small particles are shown by the filled, solid and dotted cycles. The molecules composed of large particles interact with all kinds of the molecules. On the contrary, the molecules composed of small particles are only interact with the molecules of the same kind and molecules composed of large particles, the others transparent each other.

dynamic glass transition point. Note that the decoupling of the dynamical transition density can be captured even by this formalism since the dynamical transition occurs in a replica symmetric (RS) phase, see Appendix D.

4.4 2RSB Ansatz

Recently, the similar polyamorphism as in the binary mixtures was studied in a two-component version of the spin glass model, where the two-step replica symmetry breaking (2RSB) is shown to be the key for its description [102]. This hints the following physical mechanism of the polyamorphism in binary mixtures: the free-energy landscape of the binary mixtures is divided into the multi-valley structure due to the configurations of large particles, and each of valley is further divided into the multi-valley structure due to the configurations of small particles as shown in FIG. 4.1 right. If this is the case, there should appear two distinct glass states. (i) 1RSB state: The system is trapped in a minimum in the intermediate level of the hierarchy but still can travel between the minima in the lowest level of the hierarchy. This corresponds to the state where only the large particles are frozen while small particles are mobile. (ii) 2RSB state: The system is trapped in a minimum in the lowest level of the hierarchy, where all particles are frozen.

In order to consider this possibility, one should develop the corresponding 2RSB ansatz and judge if it gives a more stable solution than the conventional 1RSB does, or not. Note that the 2RSB ansatz required here is different from the one introduced recently for the jamming transition [88] because in the present case two hierarchies corresponds to the liquid and frozen states, respectively. To this end, we introduce the following specific form of the 2RSB ansatz. We divide m replicas into m/m_1 sub-groups each of which contains m_1 replicas. The m_1 copies of small particles belonging in a same sub-group are constrained around their center of mass, whereas the copies of different sub-groups can move independently. For large particle, however, we assume that all m copies are constrained around their center of mass. In other words, the system contains $1 + m/m_1$ kinds of "molecules", namely, the molecule composed of m large particles and m/m_1 kinds of molecules composed of m_1 small particles belonging into the same sub-group. The m/m_1 kinds of small molecules only interact with the molecules of the same kind and the molecules composed of large particles, the others transparent each other. The schematic configuration of this "molecular system" is shown in FIG. 4.2.

Having this ansatz, one can write down the virial expansion of the free energy of the replica liquid starting from the standard definition of the grand canonical partition function (see Appendix C for details):

$$\begin{aligned}
\frac{\log Z_m}{N} &= \int d\overline{x}\rho_L(\overline{x})(1-\log\rho_L(\overline{x})) \\
&+ \sum_{k=1}^{m/m_1}\int d\underline{x}^k\rho_{S_k}(\underline{x}^k)(1-\log\rho_{S_k}(\underline{x}^k)) + \frac{1}{2}\int d\overline{x}d\overline{y}\rho_L(\overline{x})\rho_L(\overline{y})f_{LL}(\overline{x}-\overline{y}) \\
&+ \sum_{k=1}^{m/m_1}\frac{1}{2}\int d\underline{x}^k d\underline{y}^k\rho_{S_k}(\underline{x}^k)\rho_{S_k}(\underline{y}^k)f_{SS}(\underline{x}^k-\underline{y}^k) \\
&+ \sum_{k=1}^{m/m_1}\int d\overline{x}d\underline{y}^k\rho_L(\overline{x})\rho_{S_k}(\underline{y}^k)f_{LS}(\underline{x}^k-\underline{y}^k) \\
&+ O(\rho_L^3,\rho_{S_k}^3),
\end{aligned} \tag{4.3}$$

where ρ_L and ρ_{S_k} denote the density field of large particles and of small particles belonging into k-th sub-group, respectively. $\overline{x} = \{x^1,\cdots,x^m\}$ and $\underline{x}^k = \{x^a | a \in B_k\}$ represent the sets of the configurations in the replica space, where $B_k = \{(k-1)\times m_1 + 1,\cdots,k\times m_1\}$ denotes the set of the replicas

belonging into k-th sub-group. The Mayer functions are defined as

$$
\begin{aligned}
f_{LL}(\overline{x}-\overline{y}) &= \prod_{a=1}^{m} e^{-\beta v_{LL}(x^a-y^a)} - 1, \\
f_{LS}(\underline{x}^k-\underline{y}^k) &= \prod_{a\in B_k} e^{-\beta v_{LS}(x^a-y^a)} - 1, \\
f_{SS}(\underline{x}^k-\underline{y}^k) &= \prod_{a\in B_k} e^{-\beta v_{SS}(x^a-y^a)} - 1.
\end{aligned} \tag{4.4}
$$

The first and second terms of eq. (4.3) represent the ideal gas terms, and 3-th, 4-th and 5-th terms are represent the interactions between large molecules, small molecules, and large and small molecules, respectively [22]. We assume that $\rho_L(\overline{x})$ and $\rho_{S_k}(\underline{x}^k)$ are following the Gauusian distribution as proposed by G. Parisi and F. Zamponi [22].

4.5 Thermodynamic phase diagram

Taking the high dimensional limit, one can obtain the asymptotic expression of the free-energy and obtain the dynamical and thermodynamic glass transition points, φ_d and φ_K [22]. Here we focus on φ_K and the results for φ_d is presented in Appendix D. Near φ_K, we obtain an extremely simple expression for the free-energy:

$$
\begin{aligned}
\frac{\log Z_m}{Nm} &= g_1(m) + g_2(m_1) - d\log d + O(d\log\log d), \\
g_1(m) &= \frac{1}{m}\left[\frac{1-x}{1-x+xe^r}\frac{d}{2}\log d - \frac{2^d\varphi}{2}\frac{(1-x)^2}{1-x+xe^r}I(m)\right], \\
g_2(m_1) &= \frac{1}{m_1}\left[\frac{xe^r}{1-x+xe^r}\frac{d}{2}\log d \right. \\
&\quad \left. - \frac{2^d\varphi}{2}\frac{x^2e^r+2x(1-x)e^{r/2}}{1-x+xe^r}I(m_1)\right],
\end{aligned} \tag{4.5}
$$

with

$$
I(x) = \int_{-\infty}^{\infty} dh e^h \left[1 - e^{-x\hat{\beta}\hat{\phi}(h)}\right]. \tag{4.6}
$$

Note that this free energy reduces to the one for the conventional RLT when $m = m_1$ (see Appendix A).

The description of the state is obtained by optimizing the free energy above with respect to m and m_1. $m = m_1 = 1$ corresponds to the liquid phase. In the glass phase, contrary, m and m_1 are smaller than unity. There are two possibility, namely, $m < m_1 < 1$ and $m = m_1 < 1$. In case $m < m_1 < 1$, the glass phase is described by the 2RSB free-energy, eq. (4.3) and the values of m and m_1 are determined by the saddle point equations:

$$\begin{aligned} \frac{h(m)}{h(1)} &= \frac{1}{\hat{\varphi}(1-x)}, \\ \frac{h(m_1)}{h(1)} &= \frac{1}{\hat{\varphi}\left[x + 2(1-x)e^{-r/2}\right]}, \end{aligned} \tag{4.7}$$

with $\hat{\varphi} = \varphi/\varphi_K^{\rm mono}$ and $h(x) = -x^2\partial_x(I(x)/x)$. $\varphi_K^{\rm mono} = 2^{-d}d\log d/h(1)$ is the glass transition density of the one-component system. The glass transition density for large particles is obtained by putting $m = 1$ into eq. (4.7) above as

$$\hat{\varphi}_K^{\rm 1RSB}(x) = \frac{\varphi_K^{\rm 1RSB}(x)}{\varphi_K^{\rm mono}} = \frac{1}{1-x}. \tag{4.8}$$

Similarly, putting $m_1 = 1$ into eq. (4.7) below, we obtain the glass transition density for small particles as

$$\hat{\varphi}_K^{\rm 2RSB}(x) = \frac{\varphi_K^{\rm 2RSB}(x)}{\varphi_K^{\rm mono}} = \frac{1}{x + 2(1-x)e^{-r/2}}. \tag{4.9}$$

On the contrary, in case $m = m_1 < 1$, the glass phase is described by the 1RSB free-energy (see Appendix B). The 1RSB and 2RSB free-energy have the same value if the relative density of small particle takes the critical value,

$$x_c(r) = \frac{1 - 2e^{-r/2}}{2(1 - e^{-r/2})}. \tag{4.10}$$

When $x < x_c$, the 2RSB free-energy is more stable and when $x > x_c$, the 1RSB free-energy is more stable. Note that if $r < r_c = 2\log 2$, $x_c(r)$ is negative and there is only 1RSB phase in the phase diagram, thus $r > r_c$ is the necessary condition for arising 2RSB phase.

Combined above analysis, one can decide the full phase diagram. When the size ratio is smaller than the critical value $r < r_c = 2\log 2$, the system is described by the 1RSB ansatz and there exist only a single 1RSB glass phase.

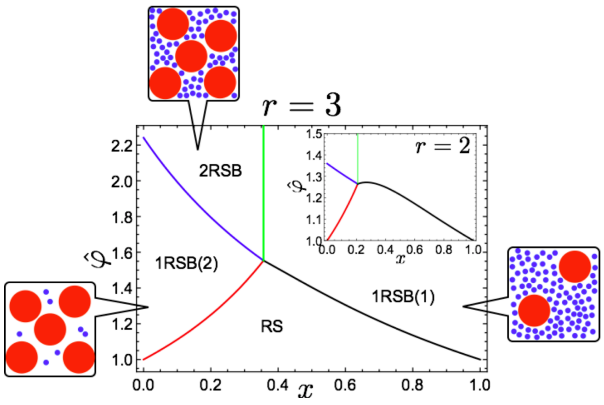

Figure 4.3: 2RSB phase diagram: The main panel is the phase diagram for $r = 3$ and the inset is for $r = 2$. The circles in the ballons represent the schematic configuration of large and small particles.

When $r > r_c$, the phase diagram has the four different phase classified by the values of m and m_1, see FIG. 4.3. For the sufficiently low density region, the solution with $m = m_1 = 1$ is the most stable and the system is in the RS phase in which all particles are mobile and the system is in the fluid phase. For the high x and high $\hat{\varphi}$ region, the solution with $m = m_1 < 1$ is the most stable and the system is in the 1RSB phase where all particles are frozen. We refer to it as the 1RSB(1). In the 1RSB(1) phase. This glass phase is stabilized mainly by the freezing of the small particles (see the right balloon of the FIG. 4.3). For the low x and moderately high $\hat{\varphi}$, the another 1RSB phase arises in which $m < m_1 = 1$ and only large particles are frozen wheres the small particles are mobile. We refer to it as the 1RSB(2). At low x and high $\hat{\varphi}$, $m < m_1 < 1$, the system is in the 2RSB phase in which all particles are frozen.

4.6 Configurational entropy

To illustrate the nature of the transitions, we also calculate the configurational entropy, Σ. In the case of the 2RSB free-energy, Σ is estimated by the

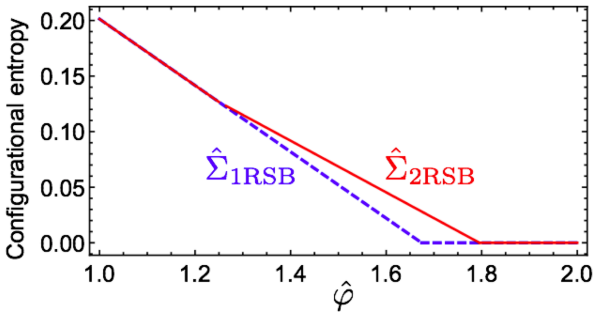

Figure 4.4: The density dependence of the configurational entropy for $r = 3$ and $x = 0.2$: The solid line represents the 2RSB result and the dashed line represents the 1RSB result.

following formula [107]:

$$\begin{aligned} \Sigma_{\rm 2RSB} &= \Sigma_1 + \Sigma_2, \\ \Sigma_1 &= -m^2 \frac{\partial}{\partial m}\left(\frac{\log Z_m}{mN}\right), \\ \Sigma_2 &= -m_1^2 \frac{\partial^2}{\partial m_1 \partial m}\left(\frac{\log Z_m}{N}\right), \end{aligned} \tag{4.11}$$

where Σ_1 represents the contribution from the number of the minima in the intermediate level of hierarchy, namely the configurations of large particles and Σ_2 represents the contribution from the number of minima in the lowest level of hierarchy, namely the configurations of small particles. Substituting the asymptotic expression of the free-energy, eq. (4.5), into above expression one can evaluate $\Sigma_{\rm 2RSB}$. In FIG. 4.4, we show the density dependence of the normalized complexity, $\hat{\Sigma}_{\rm 2RSB} = \Sigma_{\rm 2RSB}/d\log d$, at $(r, x) = (3, 0.2)$ with the solid line. For a reference, we also show the (metas-table) 1RSB result with the dashed line. From this figure, one can see that there are two bending points. The first bending occurs at $\hat{\varphi}_K^{\rm 1RSB}$, where the configurational entropy due to large particles vanishes, $\Sigma_1 = 0$. The second bending occurs at $\hat{\varphi}_K^{\rm 2RSB}$, where the configurational entropy due to small particles vanishes, $\Sigma_2 = 0$.

4.7 Summary and discussion

In summary, we developed the new 2RSB formalism of the RLT for the binary mixtures of large and small Harmonic spheres which enabled to determine the phase diagram consists of multiple glass phases. We found that when the size ratio of large and small particles is larger than the critical value, the hierarchical energy landscape emerges and the decoupling of the glass transition of large and small particles takes place. As a consequence, there arise three distinct glass phases, those are referred to as the 1RSB(1), 1RSB(2) and 2RSB phases. When the fraction of small particles, x, is relatively high, there arises 1RSB(1) in which both large and small particles are frozen. The 1RSB(1) might be stabilized by the interaction with small particles and those glasses are called as the "asymmetric glass" in terms of colloidal experiments [68, 91]. For the low x and moderately high density, there arises the 1RSB(2) phase in which only large particles are frozen whereas small particles are still mobile. For the relatively low x and high density, the 2RSB phase emerges in which both large and small particles are frozen. The predicted phase behaviors are qualitatively consistent with previous experimental and numarical results [23–26, 68] and has similarities with the dynamical transition densities predicted by the MCT [69].

One of the most significant insight among our results is the emergence of the 2RSB phase which is tantamount to the two-step hierarchical structure of the free-energy landscape. It should be interesting to directly probe this hierarchical structure in experiments and/or simulations. We guess that the rheological measurement is a good candidate for this purpose [66, 108–110]; Interestingly it is reported that the anomalous two-step yielding takes place in binary mixtures in the parameter range corresponding to the 2RSB phase [67].

The extension our results to finite dimension is the important future research target. We also believe that our higher order replica symmetry breaking picture are not restricted for the binary mixtures of disparate size ratios, but can be adapted for other polyamorphism especially originated from the decoupling of the glass transitions of the degrees of freedom. These extensions of our results are left for the future work.

Chapter 5

A paradox of the replica liquid theory of binary mixtures in the one-component limit

5.1 Introduction

As discussed in Ch. 2, the replica liquid theory (RLT) is a mean-field thermodynamic theory of the glass transition of supercooled liquids [22]. The theory was first developed for one-component monatomic systems. The RLT enables one to predict the ideal glass transition temperature, T_K, from a first-principles calculation, by considering the m replicas of the original system [22]. Thermodynamic properties near T_K are deduced by computing the free energy of a liquid consisting of m-atomic replica molecules and then taking the limit of $m \to 1$ at the end of the calculation (see Fig. 5.1 (a)).

The RLT was later extended to binary systems [98, 100]. However, it has been known that the binary RLT is *inconsistent* with its one-component counterpart. As discussed below,this contradiction originates from the assumption that each replica molecule consists of m-atoms of the *same* species (see Fig. 5.1 (b)) [98]. The molecules consisting of the atoms of the same species are identical. Thus, the Gibbs factor of the molecular system is

$$G_{2com} = N_1!N_2!, \tag{5.1}$$

where $N_1 = Nc_1$ and $N_2 = Nc_2$ denote the number of atoms of the 1-th and 2-th species, respectively. On the contrary, the Gibbs factor of the one-

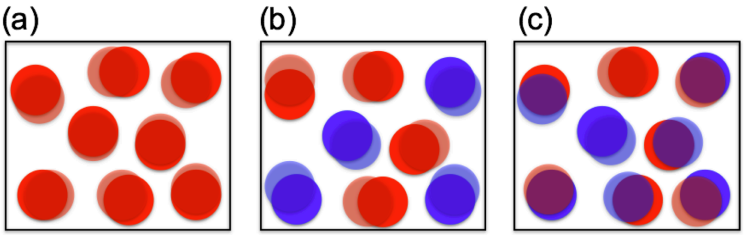

Figure 5.1: The schematic picture of the molecular system considered in the RLT: The particles of different species are denoted by different colors (blue or red). (a) The molecular system considered in the one-component RLT. (b) The molecular system considered in the conventional binary RLT, where each molecule consists of only red or blue particles. (c) The molecular system considered in our binary RLT, where each molecule consists of both red and blue particles in the weights proportional to the number fractions.

component system described in Fig.5.1 (a) is

$$G_{1com} = N!. \tag{5.2}$$

The difference between G_1 and G_2 gives the mixing entropy:

$$S_{mix} = \log G_{2com} - \log G_{1com} = c_1 \log c_1 + c_2 \log c_2, \tag{5.3}$$

where we chose the unit system so that the Boltzmann constant is one, $k_B = 1$. Note that S_{mix} sorely depends on the number fractions, c_1 and c_2, and remains finite even in the limit that the atoms of the 1-th and 2-th species are identical. Accordingly, the configurational entropy and also the glass transition point of the binary mixture are different from that of the one-component system. The binary RLT is inconsistent with that of the one-component one.

From the physical point of view, to consider the system as described in Fig. 5.1 (b) is tantamount to assume that a permutation of atoms of one species with atoms of the other species in a given glass configuration is forbidden [98]. This is indeed the case if, say, the atomic radii of the two species are very different. Clearly this assumption is inappropriate if the two species are very similar or exactly identical because a permutation of the atoms of different species are allowed. Concomitantly, one should consider the molecular system where each molecule consists of the atoms of

different species with the weight proportional to the number fractions, as shown in Fig. 5.1 (c). In this chapter, we reformulate the RLT so as to describe the molecular system described in Fig. 5.1 (c) and show that with this reformulation, the inconsistency between the RLT of one-component system and binary mixtures is resolved.

5.2 Theory

We consider a binary liquid composed of A and B atoms. The important step is to rewrite the expression of the grand canonical partition function in a form discussed by Morita and Hiroike [111] as

$$Z = \sum_{N=0}^{\infty} \frac{1}{N!} \prod_{i=1}^{N} \sum_{\nu_i \in \{A,B\}} \int d\boldsymbol{x}_i \exp\left[-\beta V_N + \beta \sum_{i=1}^{N} \mu_{\nu_i} \right], \tag{5.4}$$

where β is the inverse temperature, N is the total number of atoms, V_N is the total potential energy. $\boldsymbol{x}_i$, $\nu_i \in \{A, B\}$, and μ_{ν_i} are the position, species, and chemical potential of i-th atoms, respectively. Eq. (5.4) is mathematically equivalent to the standard expression for Z [11]. This expression can be readily generalized to the replicated liquid consisting of m-atomic replica molecules as

$$\begin{aligned} Z_m = \sum_{N=0}^{\infty} \frac{1}{N!} \prod_{i=1}^{N} \left(\prod_{a=1}^{m} \sum_{\nu_i^a \in \{A,B\}} \int d\boldsymbol{x}_i^a \right) \\ \times \exp\left[-\beta \sum_{a=1}^{m} V_N^a + \beta \sum_{i=1}^{N} \psi_{\overline{\nu}_i}(\overline{\boldsymbol{x}}_i) \right], \end{aligned} \tag{5.5}$$

where $\psi_{\overline{\nu}_i}(\overline{\boldsymbol{x}}_i) \equiv \sum_{a=1}^{m} \mu_{\nu_i^a} - u_{\overline{\nu}_i}(\overline{\boldsymbol{x}}_i)$ is the generalized chemical potential in which the external potential $u_{\overline{\nu}_i}(\overline{\boldsymbol{x}}_i)$ is included. $\overline{\boldsymbol{x}}_i \equiv (\boldsymbol{x}_i^1, \cdots, \boldsymbol{x}_i^m)$ and $\overline{\nu}_i \equiv (\nu_i^1, \cdots, \nu_i^m)$ denote the set of the positions and components of m atoms of the i-th molecule. The advantage to express Z_m à la Morita-Hiroike as Eq. (5.5) is that assigning a label of the component $\overline{\nu}_i$ to each atom enables one to describe replica molecules consisting of different set of species. The

density field conjugated to $\psi_{\overline{\nu}}(\overline{x})$ can be written as

$$\rho_{\overline{\nu}}(\overline{\boldsymbol{x}}) = \sum_{i=1}^{N} \left\langle \prod_{a=1}^{m} \delta(\boldsymbol{x}^a - \boldsymbol{x}_i^a)\delta_{\nu_i^a,\nu_i^a} \right\rangle = \frac{\delta \log Z_m}{\delta \psi_{\overline{\nu}}(\overline{\boldsymbol{x}})}. \tag{5.6}$$

Following the standard procedure [11], one can express the free energy, $-\beta F$, by the Legendre transformation from $\psi_{\overline{\nu}}(\overline{\boldsymbol{x}})$ to $\rho_{\overline{\nu}}(\overline{\boldsymbol{x}})$, which can be written as the sum of the ideal and the excess parts;

$$\beta F[\rho_{\overline{\nu}}(\overline{\boldsymbol{x}})] = -\sum_{\overline{\nu}} \int d\overline{\boldsymbol{x}} \rho_{\overline{\nu}}(\overline{\boldsymbol{x}})(1 - \log \rho_{\overline{\nu}}(\overline{\boldsymbol{x}})) + \beta F_{\rm ex}[\rho_{\overline{\nu}}(\overline{\boldsymbol{x}})]. \tag{5.7}$$

The equilibrium free energy is obtained by minimizing Eq. (5.7) with respect to the density profile $\rho_{\overline{\nu}}(\overline{\boldsymbol{x}})$. For one-component systems, the standard procedure is to assume that $\rho_{\overline{\nu}}(\overline{\boldsymbol{x}})$ is Gaussian-shaped and use its width, or the cage size, as the minimization parameter [22]. Once the equilibrium free energy is obtained, S_c is calculated by $S_c = \lim_{m\to 1} m^2 \frac{\partial}{\partial m} \frac{\beta F}{mN}$. The ideal glass transition temperature, T_K, is identified as the point at which S_c vanishes [22]. For binary liquids, however, the full computation is a challenging task because the cage sizes vary depending on the components $\overline{\nu}$. But, at least, one can demonstrate that the one-component result is correctly derived in the limit that atoms of two components are identical or very similar. In this limit, the density profile in the replica space can be written as

$$\rho_{\overline{\nu}}(\overline{\boldsymbol{x}}) = \rho \int d\boldsymbol{X} \prod_{a=1}^{m} \left(\sum_{\mu} c_\mu \delta_{\mu\nu^a} \gamma_{\Delta_\mu}(\boldsymbol{x}^a - \boldsymbol{X}) \right), \tag{5.8}$$

where $\gamma_A(\boldsymbol{x} - \boldsymbol{X}) = e^{-|\boldsymbol{x}-\boldsymbol{X}|^2/2\Delta}/(4\pi\Delta)^{d/2}$ is the Gaussian function centered at a reference position $\boldsymbol{X}$ with the cage size $\sqrt{\Delta}$. $\rho = N/V$ is the number density, and $c_\nu = N_\nu/N$ is the number fraction of the $\nu \in \{A, B\}$ species. Eq. (5.8) expresses that atoms of different species constitute a single replica molecules with the composition ratio of $c_A : c_B$. This ansatz corresponds to the limit where a permutation of the atoms of different species are allowed in a given glass configuration. The difference of the free energy from that of the one-component system F_1 is expressed by the difference in the ideal gas

part (since the excess parts are identical in this limit) as

$$\begin{aligned}\beta\Delta F &\equiv \beta\left\{F[\rho_{\overline{\nu}}] - F_1[\rho]\right\} \\ &= -\sum_{\overline{\nu}} \int d\overline{\boldsymbol{x}} \rho_{\overline{\nu}}(\overline{\boldsymbol{x}})(1 - \log \rho_{\overline{\nu}}(\overline{\boldsymbol{x}})) \\ &+ \int d\overline{\boldsymbol{x}} \rho(\overline{\boldsymbol{x}})(1 - \log \rho(\overline{\boldsymbol{x}})),\end{aligned} \tag{5.9}$$

where $\rho(\overline{\boldsymbol{x}})$ is the density profile of the one-component system. Because $\rho_{\overline{\nu}}(\overline{\boldsymbol{x}}) = \rho(\overline{\boldsymbol{x}}) \times (\prod_a c_{\nu^a})$ in the one-component limit, we arrive at $\beta\Delta F = mN \sum_\mu c_\mu \log c_\mu$. This implies that the S_c of the binary RLT correctly converges to that of the one-component $S_{c,1}$, because $\Delta S_c \equiv S_c - S_{c,1} = m^2 \partial_m \left(\beta\Delta F/mN\right) = 0$.

In the opposite limit where the atoms of the two species are very different and one replica molecule consists of atoms solely of the one species, one can show that the previous results of binary RLT [100] are recovered. In this case, the density profile should be written as

$$\rho'_{\overline{\nu}}(\overline{\boldsymbol{x}}) = \rho \int d\boldsymbol{X} \sum_\mu c_\mu \left(\prod_{a=1}^{m} \delta_{\mu\nu^a} \gamma_{\Delta_\mu}(\boldsymbol{x}^a - \boldsymbol{X}) \right). \tag{5.10}$$

Note the difference from Eq. (5.8); The order of the product over the atoms a and the summation over the species μ have been exchanged. Due to the factor $(\prod_a \delta_{\mu\nu^a})$ in Eq. (5.10), $\rho'_{\overline{\nu}}(\overline{\boldsymbol{x}})$ vanishes unless each molecule consists of a single species. The non-vanishing component of the density profile is $c_\nu \rho \int d\boldsymbol{X} \prod_a \gamma_{\Delta_\nu}(\boldsymbol{x}^a - \boldsymbol{X})$ ($\nu =$ A or B), which is exactly the density field employed in previous studies of the binary RLT [100]. Eq. (5.10) should not be used in the one-component limit because it gives a solution which is less stable than Eq. (5.8): Substituting Eq. (5.10) into Eq. (5.7) and optimizing the parameter Δ_ν, one finds $\beta\Delta F = N \sum_\mu c_\mu \log c_\mu$, which is larger than $\beta\Delta F$ from Eq. (5.8)[1]. This solution also leads to a pathological result $\Delta S_c = -\sum_\mu c_\mu \log c_\mu > 0$; that is, S_c calculated assuming Eq. (5.10) is larger than the correct one-component configurational entropy by the mixing entropy [112].

[1]Exchange "larger" with "smaller" for $m < 1$, see Ref. [22].

5.3 Conclusion

In summary, we reformulate the RLT of binary, or multi-component mixtures, which correctly accounts for a permutation of the atoms in a glass configuration and show that it resolves the inconsistency between the one-component RLT and the binary RLT. The binary RLT in the previous studies is valid only in the limit where the atoms of different species are so different that a permutation of the atoms of different components is forbidden. In the one-component limit, one has to consider all possible permutations of atoms and adopts the density profile expressed as Eq. (5.8) to obtain the correct configurational entropy. For general cases between these two extreme limits, the density profile should be determined so as to minimize the free energy, Eq. (5.7). Its implementation, however, may be challenging. The results discussed above imply a possibility, for example, that a binary liquid of small and large hard spheres undergoes the glass-glass transition from the *"disordered" glass* where the both types of spheres constitute a replica molecule to the *"ordered" glass* where one replica molecule consists solely of one of the component, as the size ratio between the two components is varied, much the same way as the metallic alloys undergo the order-disorder phase transition as the interactions are varied [113]. Note that this possibility has also been pointed out in Ref. [112] in the context of the numerical simulation of the multi-component mixtures. Finally, we note that the generalization to n-component system is straightforward by allowing ν_i in Eq. (5.4) to take n-different states. Polydisperse case can be obtained in the $n \to \infty$ limit with a caveat about a subtlety to take the continuous limit (see Ref. [112]).

Chapter 6

Conclusion

In this work, we have constructed a mean-field theory to describe the glass transition of binary mixtures of desperate size ratio. Our study is based on the replica liquid theory which combines the replica method used in the spin glasses with the conventional liquid theory. The ordinal replica liquid theory has been developed so as to describe the glass transition of one-component systems or the two-component systems whose size ratio is close to unity. In those cases, the glass transition is identified with the one-step replica symmetry breaking transition (1RSB) which is the simplest case among the replica symmetry breaking transitions. However, it is known that the replica liquid theory based on the 1RSB cannot describe the decoupling of the glass transitions of large and small particles. In this thesis, we have uncovered the origin of this discrepancy and proposed the new framework to remove this discrepancy.

As a fist step to this end, we have investigated the two-component version of the p-spin spherical model (PSM). The PSM is a fully connected spin glass model and since the model can be solved analytically, one can investigate the model without relying uncontrollable approximations. It has been shown that the one-component version of the PSM exhibits the 1RSB, which corresponds to the glass transition of one-component systems. However, we found that the two-component version of the PSM exhibits not only the 1RSB but also more complex two step replica symmetry breaking (2RSB) transition when the interaction strengths of the spins of the different species are well separated. Notably, the decoupling of the glass transition of the different species is concomitant with emerging of the 2RSB.

Next, we have constructed the replica liquid theory based on the 2RSB

assumption and applied the theory to the particle system. We have investigated the binary harmonic system which is a typical model system of the binary colloidal mixtures consisting of large and small particles. We obtained the phase diagram in the high dimensional limit (a mean-field limit) where the analytic calculation is available. The qualitative behavior of the phase diagram is the same with that of the two-component version of the PSM. When the size ratio between the different species is sufficiently large, the system exhibits the decoupling of the glass transition points of large and small particles. Concomitantly, the system exhibits the 2RSB transition. More concretely, the phase diagram divides into three distinct parts. The 1RSB(1) phase where both large and small particles are frozen. The 1RSB(2) phase where only large particles are frozen while small particles are mobile. The 2RSB phase where both large and small particles are frozen. The qualitative shape of the phase diagram obtained by our theoretical investigation is the same with that obtained by the colloidal experiment, though the 2RSB phase has never been discovered by the experiments yet.

Our investigation is mainly focused on the mean-field limit, namely, the high dimensional limit. The important future work is to perform the 2RSB calculation in finite dimensions and compare the quantitative value of the glass transition point with the experiments and numerical simulations. This is possible by relying the cage expansion and the hypernetted chain approximation. The calculation is now going on. Another important future work is to validate the existence of the 2RSB structure on the free-energy landscape. This may be most directly observed by calculating the dynamics of the inherent structure by the numerical simulations.

In the final chapter, we have discussed about the discrepancy between the one-component and two-component version of the replica liquid theory. We found that the mixing entropy of the molecular system considering in the one-component replica liquid theory and that of the two-component replica liquid theory differs even in the limit that the particles of the two species are identical. This implies that the glass transition point estimated by the two-component replica liquid theory is different from that obtained by the one-component counterpart even in the one-component limit. The origin of the discrepancy is that the effects of the swapping of the particles of different species are not included in the conventional two-component replica liquid theory. We have reformulated the two-component replica liquid theory so as to include this effect and showed that the reformed theory is surely consistent with the one-component replica liquid theory. Apart from the limit that the

particles of different species are identical, the effect of the swapping of the particles of different species is non trivial and investigation of this case is left for the future work.

Appendix A

Perturbation analysis of the continuous transition

In this appendix, we construct the perturbative theory around the 1RSB ansatz which allows us to calculate the continuous 2RSB thermodynamic transition temperature, $T_K^{(2c)}$. Here, we expand the saddle point equations about the differences between the 1RSB and 2RSB order parameters, $q_2 - q_1$ and $p_2 - p_1$, and derive the convenient equations to evaluate $T_K^{(2c)}$. To this end, the most convenient staring point is

$$\begin{aligned} \frac{2}{(m_2-1)c}\frac{\partial G_{2RSB}}{\partial q_2} - \frac{2}{(m_1-m_2)(1-c)}\frac{\partial G_{2RSB}}{\partial q_1} = 0, \\ \frac{2}{(m_2-1)c}\frac{\partial G_{2RSB}}{\partial q_2} - \frac{2}{(m_1-m_2)(1-c)}\frac{\partial G_{2RSB}}{\partial q_1} = 0. \end{aligned} \tag{A.1}$$

After the some manipulations, equations (A.1) can be rewritten as

$$\frac{1}{m_2}\left(\frac{1}{1-q_2^\alpha} - \frac{1}{1-(1-m_2)q_2^\alpha - m_2 q_1^\alpha}\right) = M_\alpha,\ \alpha \in \{q, p\}, \tag{A.2}$$

where $q_i^q = q_i$ and $q_i^p = p_i$. The kernels, M_q and M_p, are defined as

$$\begin{aligned} M_q &= \frac{3}{2T^2}\left\{c^2(q_2^2 - q_1^2) + 2J^2c(1-c)(q_2p_2 - q_1p_1) + J^2(1-c)^2(p_2^2 - p_1^2)\right\}, \\ M_p &= \frac{3}{2T^2}\left\{J^2c^2(q_2^2 - q_1^2) + 2J^2c(1-c)(q_2p_2 - q_1p_1) + J^2(1-c)^2(p_2^2 - p_1^2)\right\}. \end{aligned} \tag{A.3}$$

Substituting $q_2^\alpha = q_\alpha$ and $q_1^\alpha = q_\alpha - \delta q_\alpha$ into equations (A.1) and expanding $\delta q_\alpha = \varepsilon q_\alpha^{(1)} + \varepsilon^2 q_\alpha^{(2)} + O(\varepsilon^3)$, one obtains the perturbative series for ε. Below, we show that the first order term of ε decides the transition temperature and the second order provides the value of m_2 at the transition temperature.

For the first order of the perturbative expansion of equation (A.2) about ε, we obtain

$$\sum_\beta M_{\alpha,\beta} q_\beta^{(1)} = \frac{1}{(1-q_\alpha)^2} q_\alpha^{(1)}, \tag{A.4}$$

where we have defined the auxiliary matrix as

$$M_{\alpha,\beta} = -\left.\frac{\partial M_\alpha}{\partial q_1^\beta}\right|_{\{q_2^\gamma = q_1^\gamma = q^\gamma\}}. \tag{A.5}$$

The necessary condition that the equation (A.4) has the non-zero solution is

$$M_{q,p} M_{p,q} = \left(M_{q,q} - \frac{1}{(1-q)^2}\right)\left(M_{p,p} - \frac{1}{(1-p)^2}\right). \tag{A.6}$$

This is the closed equation for q, p and the temperature T. Substituting the 1RSB result for q and p, we can solve equation (A.6) for T and obtain $T_K^{(2c)}$. As shown in Figure 3.5, at $T_K^{(2c)}$, the m_2 changes discontinuously from 1 to some positive value smaller than 1. This value of m_2 can be obtained by the second order term of ε:

$$\frac{1}{(1-q_\alpha)^2} q_\alpha^{(2)} - \frac{m_2}{(1-q_\alpha)^3} (q_\alpha^{(1)})^2 = \sum_{\alpha\beta} M_{\alpha,\beta} q_\beta^{(2)} + \sum_{\alpha\beta} M_{\alpha,\beta\gamma} q_\beta^{(1)} q_\gamma^{(1)}, \tag{A.7}$$

where we have defined

$$M_{a,\beta\gamma} = \frac{1}{2}\left.\frac{\partial^2 M_\alpha}{\partial q_1^\beta \partial q_1^\gamma}\right|_{\{q_2^\gamma = q_1^\gamma = q^\gamma\}}. \tag{A.8}$$

Note that equation (A.7) depends on $q_\alpha^{(2)}$, the value of which is undecided at present. To remove the terms which contains $q_\alpha^{(2)}$ from equation (A.7), inspired by the perturbative analysis of the MCT [3], we introduce the left eigen vector, l_α, which satisfies

$$\sum_\beta M_{\alpha,\beta} l_\beta = \frac{1}{(1-q_\alpha)^2} l_\alpha. \tag{A.9}$$

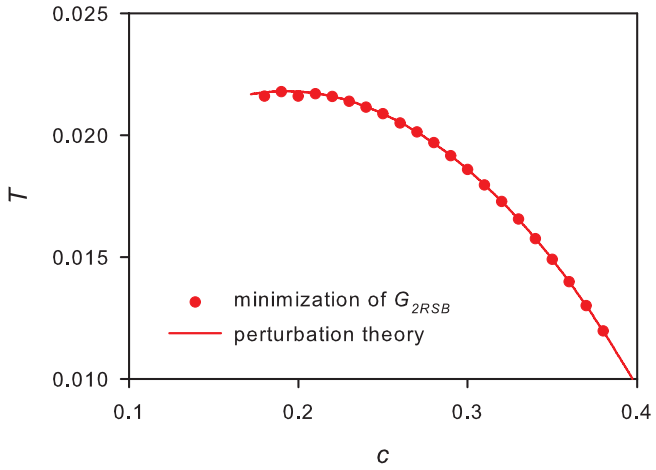

Figure A.1: The continuous 2RSB transition temperatures $T_K^{(2c)}$ calculated by the minimization of G_{2RSB} (symbols) and equation (A.6) (line) at $J = 0.03$.

Using this, $q_\alpha^{(1)}$ can be expressed as

$$q_\alpha^{(1)} = g l_\alpha, \tag{A.10}$$

where g is a constant. Also, we introduce the right eigen vector by

$$\sum_\alpha r_\alpha M_{\alpha,\beta} = \frac{1}{(1-q_\beta)^2} r_\beta. \tag{A.11}$$

Multiplying $\sum_\alpha r_\alpha$ from the left of equation (A.7) and using equation (A.10), we finally reach the compact formula for m_2:

$$m_2 = -\frac{\sum_{\alpha\beta\gamma} r_\alpha M_{\alpha,\beta\gamma} l_\beta l_\gamma}{\sum_\alpha r_\alpha l_\alpha^2 (1-q_\alpha)^{-3}}. \tag{A.12}$$

From this expression, it is clear that the value of m_2 is independent from the normalization constants of the eigen vectors, equation (A.9) and equation (A.11). The right hand side of equation (A.12) is the function of q, p, and T. Substituting the 1RSB results into q and p and $T_K^{(2c)}$ calculated by equation (A.6) into T, we obtain the value of m_2.

An advantage of the formalism constructed above is that one can evaluate $T_K^{(2c)}$ and the value of m_2 at the transition point with only the information about the 1RSB result. This enables a more precise investigation of the

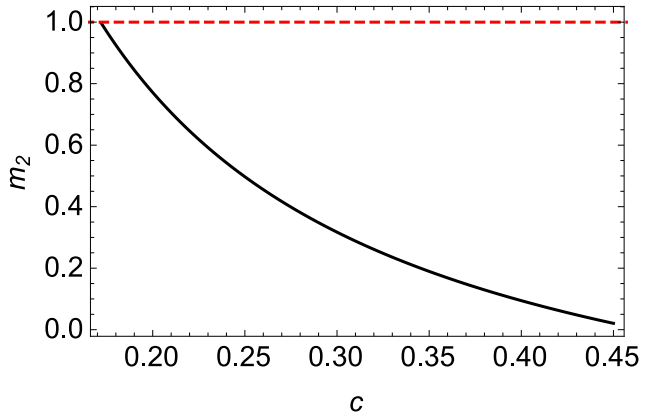

Figure A.2: The value of m_2 on the continuous 2RSB transition line $T_K^{(2c)}$ at $J = 0.03$

phase behavior than that of the full numerical minimization of G_{2RSB}. In Figure A.1, we compare $T_K^{(2c)}$ calculated by equation (A.6) with that calculated by the minimization of G_{2RSB} (as in Figure. 3.4). They are almost identical.

To determine the critical point at which the continuous transition ceases to exist and the transition becomes discontinuous, one should observe the value of $m_2(c)$. In Figure A.2, we show the c dependence of $m_2(c)$ calculated by equation (A.12) on $T_K^{(2c)}(c)$. The value of m_2 increases with decreasing c and reaches $m_2 = 1$ at the critical point c_c= 0.17174, where $T_K^{(2c)}(c_c) = T_c = 0.021667$. Note that $m_2 = 1$ is a signal of the discontinuous transition, therefore it is natural to guess that at $c = c_c$, the continuous 2RSB thermodynamic transition line, $T_K^{(2c)}(c)$, is connected to the discontinuous 2RSB thermodynamic and dynamical transition lines, $T_d^{(2)}(c)$ and $T_K^{(2d)}(c)$. This assumption is indeed correct, see Figure 3.4.

Appendix B

1RSB thermodynamic phase diagram

Here, we present the results with the conventional RLT based on the one-step replica symmetric breaking (1RSB) assumption [22,39,97,100], and show that the partially frozen phase can not be described by this theory. Following the strategy of Ref. [22], we introduce the density distribution function in replica space as

$$\rho_L(\overline{x}) = \sum_{i\in\text{Large}} \left\langle \prod_{a=1}^{m} \delta(x^a - x_i^a) \right\rangle, \ \rho_S(\overline{x}) = \sum_{i\in\text{Small}} \left\langle \prod_{a=1}^{m} \delta(x^a - x_i^a) \right\rangle, \quad \text{(B.1)}$$

where $\overline{x} = \{x^1, \cdots, x^m\}$ represents the set of the particle positions in the replica space. Expanding the free-energy of the replicated system by $\rho_L(\overline{x})$ and $\rho_S(\overline{x})$, we obtain a series of perturbative expansion [22, 100]:

$$\begin{aligned} \log Z_m &= S_{id} + S_{int}, \\ S_{id} &= \sum_{\mu\in\{L,S\}} \int d\overline{x} \rho_\mu(\overline{x})(1 - \log \rho_\mu(\overline{x})), \\ S_{int} &= \sum_{\mu\nu\in\{L,S\}} \frac{1}{2} \int d\overline{x} d\overline{y} \rho_\mu(\overline{x}) \rho_\nu(\overline{y}) f_{\mu\nu}(\overline{x} - \overline{y}) + O(\rho_L^3, \rho_S^3), \end{aligned} \quad \text{(B.2)}$$

where the Mayer functions are defined as

$$f_{\mu\nu}(\overline{x} - \overline{y}) = \prod_{a=1}^{m} e^{-\beta v_{\mu\nu}(x^a - y^a)} - 1. \quad \text{(B.3)}$$

Note that the 1RSB free-energy, eq. (B.2), also obtained by substituting $m = m_1$ into the 2RSB free-energy, eq. (4.3).

Now, we assume the 1RSB Gussian ansatzs [22, 100]:

$$\rho_\mu(\overline{x}) = \rho_\mu \int dX \prod_{a=1}^{m} \gamma_{A_\mu}(x^a - X), \tag{B.4}$$

where $\gamma_A(x)$ is the normal distribution function whose variance is A. Putting eq. (B.4) into eq. (B.2), it is straight forward to show that

$$\begin{aligned} S_{id} &= \sum_\mu N_\mu \left[1 - \log \rho_\mu - \frac{d}{2}(1-m)\log 2\pi A_\mu - \frac{d}{2}(1 - m - \log m) \right], \\ S_{int} &= \frac{1}{2} \sum_{\mu\nu} \frac{N_\mu N_\nu}{V} \int dr \left(q^m_{\mu\nu}(r) - 1 \right), \end{aligned} \tag{B.5}$$

with

$$q_{\mu\nu}(r) = \int dR \gamma_{A_\mu + A_\nu}(r+R) e^{-\beta v_{\mu\nu}(R)}. \tag{B.6}$$

It is known that in the high dimensional limit, the thermodynamic glass transition density scales as $\varphi_K = O(2^{-d} d \log d)$ and the cage size scales as $A = O(1/d^2 \log d)$ [22]. Thus, one can see that $\gamma_A(x) \sim \delta(x)$ and $q_{\mu\nu}(r) \sim e^{-\beta v_{\mu\nu}(r)}$ since A shrinks to zero. Substituting this into eq. (B.5), we obtain the asymptotic form of the free-energy near the thermodynamic glass transition point,

$$\frac{\log Z_m}{Nm} = \frac{1}{m} \left[\frac{d}{2} \log d - \frac{\varphi}{2} \frac{(1 - x + x e^{r/2})^2}{1 - x + x e^r} I(m) \right] - d \log d + O(d \log \log d), \tag{B.7}$$

where $I(m)$ is defined as eq. (4.6). The value of m should be determined by the saddle point equation, expressly,

$$\hat{\varphi}_K(x) = \frac{\varphi_K(x)}{\varphi_K^{\text{mono}}} = \frac{1 - x + x e^r}{(1 - x + x e^{r/2})^2}, \tag{B.8}$$

where φ_K^{mono} denotes the glass transition point for the one-component system ($x = 0$ or $x = 1$). The decoupling of large and small particles is not captured by the 1RSB ansatz, since there are only fluid phase (RS) and fully frozen phase (1RSB). Typical phase diagrams /predicted by eq. B.8 are shown in FIG. (**??**).

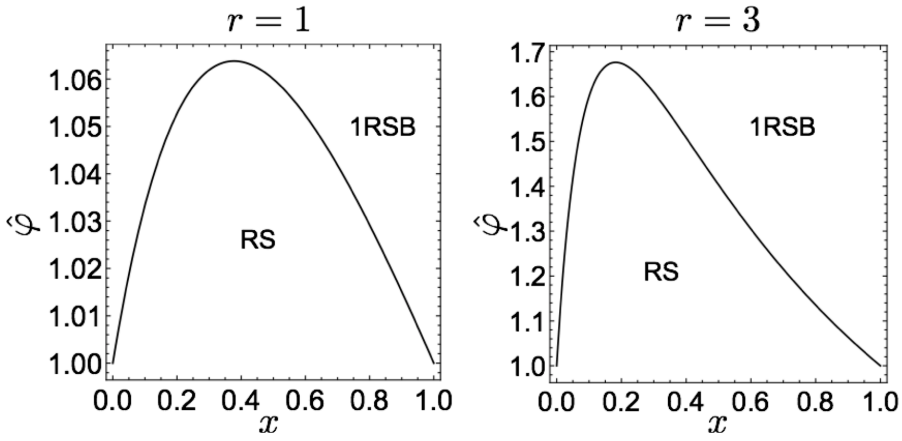

Figure B.1: 1RSB phase diagram

Appendix C

Derivation of eq. (4.3)

The grand canonical partition function of the molecular system as shown in FIG. (4.2) is

$$Z_m = \left(\sum_{N_L=0}^{\infty} \frac{1}{N_L!} \prod_{a=1}^{m} \prod_{i \in L} \int dx_i^a \right) \prod_{k=1}^{m/m_1} \left(\sum_{N_{S_k}}^{\infty} \frac{1}{N_{S_k}!} \prod_{a \in B_k} \prod_{i \in S_k} \int dx_i^a \right) \times \exp\left[-\beta \sum_{a=1}^{m} V_{LL}^a - \beta \Psi_L \right] \prod_{k=1}^{m/m_1} \exp\left[-\beta \sum_{a \in B_k} \left(V_{S_k S_k}^a + V_{L S_k}^a \right) - \beta \Psi_{S_k} \right], \tag{C.1}$$

where the subscripts L and S_k denote large particles and the small particles belonging into k-th sub-group, respectively. $B_k = \{(k-1) \times m_1 + 1, \cdots, k \times m_1\}$ denotes the set of the replicas belonging into k-th sub-group. $V_{\mu\nu}^a$ denotes the interaction potential between particles of μ and ν species. The Ψ_L and Ψ_{S_k} are the intrinsic chemical potentials [11] for the molecules, which is defined by

$$\begin{aligned} \Psi_L &= \sum_{i \in L} \psi_L(\overline{x}_i) = \sum_{i \in L} (\phi_L(\overline{x}) - \mu_L), \\ \Psi_{S_k} &= \sum_{i \in S_k} \psi_{S_k}(\underline{x}_i) = \sum_{i \in S_k} (\phi_{S_k}(\underline{x}_i^k) - \mu_{S_k}), \end{aligned} \tag{C.2}$$

where $\overline{x} = \{x^1, \cdots, x^m\}$ and $\underline{x}^k = \{x^a | a \in B_k\}$ represent the sets of the configurations in the replica space, and μ_L and μ_{S_k} represent the chemical potentials. Here, we introduced the intra-molecular interaction potentials,

$\phi_L(\overline{x})$ and $\phi_{S_k}(\underline{x}^k)$. The intrinsic chemical potentials, eqs. (C.2), allow us to calculate the one point density distribution functions for the molecules:

$$\rho_L(\overline{x}) = \sum_{i\in L} \left\langle \prod_{a=1}^{m} \delta(x^a - x_i^a) \right\rangle = \frac{\delta \log Z_m}{\delta \psi_L(\overline{x})},$$
$$\rho_{S_k}(\underline{x}^k) = \sum_{i\in S_k} \left\langle \prod_{a\in B_k} \delta(x^a - x_i^a) \right\rangle = \frac{\delta \log Z_m}{\delta \psi_{S_k}(\underline{x}^k)}. \tag{C.3}$$

One can see that the diagrams generated by this Mayer cluster expansion [11] are the same as those of the $1+m/m_1$ component non-molecular system after the densities distributions, eqs. (C.3), and the Mayer functions, eqs. (4.4), are replaced by the those of the non-molecular system [11, 111]. Calculating second order for ρ_L and ρ_{S_k}, we obtain eq. (4.3).

Appendix D

Dynamical phase diagram

In this section, we shall argue the dynamical glass transition point, φ_d, at which there arises the non-trivial solution for the cage sizes. The saddle point equations for the cage sizes are obtained from the derivation of the free-energy eq. (B.5) with respect to A_L and A_S:

$$\begin{aligned}\frac{1}{A_L} &= \frac{2}{d(1-m)}\left[\frac{\rho_L}{2}\frac{\partial}{\partial A_L}\int dr q_{LL}(r)^m + \rho_S\frac{\partial}{\partial A_S}\int dr q_{LS}(r)^m\right],\\ \frac{1}{A_S} &= \frac{2}{d(1-m)}\left[\frac{\rho_S}{2}\frac{\partial}{\partial A_S}\int dr q_{SS}(r)^m + \rho_S\frac{\partial}{\partial A_S}\int dr q_{SL}(r)^m\right].\end{aligned} \tag{D.1}$$

For simplicity, we will investigate the hard-sphere limit ($T = 0$). The asymptotic analysis for the one-component hard sphere system on the high dimensional limit [22] can be easily extended for this model and one obtain

$$\begin{aligned}\frac{1}{\hat{A}_L} &\sim \tilde{\varphi}\left[(1-x)M(\hat{A}_L) + xe^{r/2}M\left(\frac{\hat{A}_L+\hat{A}_S}{2}\right)\right],\\ \frac{1}{\hat{A}_S} &\sim \tilde{\varphi}\left[xM(\hat{A}_S) + (1-x)e^{-r/2}M\left(\frac{\hat{A}_L+\hat{A}_S}{2}\right)\right],\end{aligned} \tag{D.2}$$

where we defined $\hat{A}_\mu = d^2A_\mu/D_{\mu\mu}^2$ and $\tilde{\varphi} = 2^d\varphi/d$. The auxiliary functions are defined as

$$\begin{aligned}M(\hat{A}) &= -\int dy e^y \log\left[\Theta\left(\frac{y+\hat{A}}{\sqrt{4\hat{A}}}\right)\right]\frac{\partial}{\partial\hat{A}}\Theta\left(\frac{y+\hat{A}}{\sqrt{4\hat{A}}}\right),\\ \Theta(x) &= \frac{1}{2}\left(1+\mathrm{erf}(x)\right).\end{aligned} \tag{D.3}$$

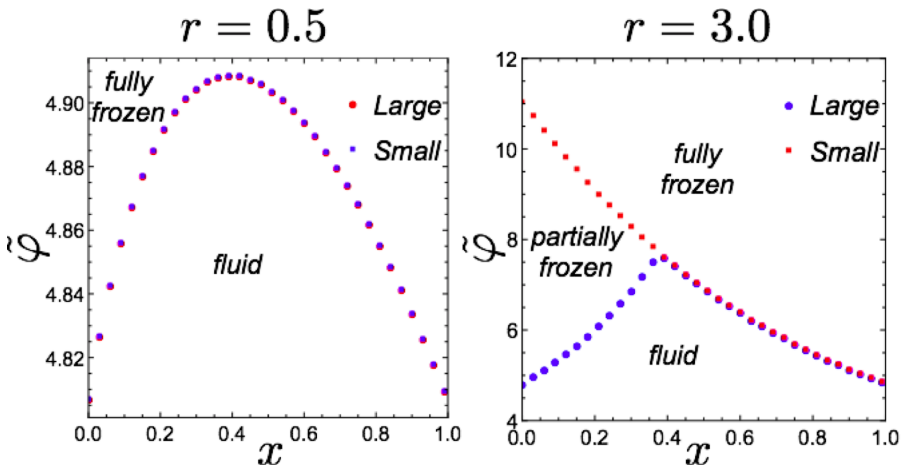

Figure D.1: Dynamic phase diagram for hard spheres: The filled cycles denote the dynamical transition points for large particles. The filled squares denote the dynamical transition points for small particles.

Solving eqs. (D.2) numerically, one obtains the cage sizes and the dynamical transition point. When the size ratio between large and small particles, r, is small, the dynamical transition of large and small particles take place simultaneously, see the LHS of FIG. D.2. Contrary, when r is sufficiently large, dynamical transition point of large and small particles can be decoupled and there arises the partially frozen phase in which only large particles are frozen ($\hat{A}_L < \infty$) whereas small particles behaves as fluid ($\hat{A}_S = \infty$), see the RHS of FIG. D.1.

Acknowledgment

I thank to all those who have supported me during my phD course.

I express my appreciation to the PhD adviser prof. Kunimasa Miyazaki for enthusiastic discussions and kidful supports.

I would also like to thank collaborators, Prof. Atushi Ikeda, Prof. Hajime Yoshino, and Prof. Giulio Biroli for academic supports during my PhD course. Without their guidance and persistent help, this thesis would not have been possible.

Special thanks to Prof. Francesco Zamponi, Prof. Koji Hukushima, Prof. Frederic van Wijland, Prof. Tomasso Rizzo, Dr. Takeshi Kawasaki, Dr. Ryoji Miyazaki, and Dr. Misaki Ozawa for their comments and discussions.

I am grateful to the members of the non-linear physics group in Nagoya University, Masaki Kajitani, Misae Hayashi and Kenta Nomoto.

Finally, I thank my family for everyday encouragement.

Bibliography

[1] P. G. Debenedetti and F. H. Stillinger, Nature **410**, 259 (2001).

[2] A. Cavagna, Phys. Rep. **476**, 51 (2009).

[3] W. Götze, *Complex Dynamics of Glass-Forming Liquids: A Mode-Coupling Theory*volume 143 (Oxford University Press, 2008).

[4] L. Berthier and G. Biroli, Rev. Mod. Phys. **83**, 587 (2011).

[5] K. Binder and W. Kob, *Glassy materials and disordered solids: An introduction to their statistical mechanics* (World Scientific, 2011).

[6] G. Biroli and J. P. Garrahan, J. Chem. Phys. **138**, 12A301 (2013).

[7] P. G. Debenedetti, *Metastable liquids: concepts and principles* (Princeton University Press, 1996).

[8] C. Angell, J. Non-Cryst. Solids **102**, 205 (1988).

[9] C. A. Angell, Science **267**, 1924 (1995).

[10] G. S. Fulcher, J. Am. Ceram. Soc. **8**, 339 (1925).

[11] J.-P. Hansen and I. R. McDonald, *Theory of simple liquids* (Elsevier, 1990).

[12] T. C. Hales, Ann. Math. **162**, 1065 (2005).

[13] T. C. Hales and S. P. Ferguson, A formulation of the kepler conjecture, in *The Kepler Conjecture*, pp. 83–133, Springer, 2011.

[14] T. Hales *et al.*, arXiv:1501.02155 (2015).

[15] R. Richert and C. Angell, J. Chem. Phys. **108**, 9016 (1998).

[16] J.-L. BARRAT, M. FEIGELMAN, and J. KURCHAN, arXiv preprint cond-mat/0212344 (2002).

[17] P. W. Anderson *et al.*, Science **177**, 393 (1972).

[18] H. Nishimori and G. Ortiz, *Elements of phase transitions and critical phenomena* (OUP Oxford, 2010).

[19] L. Berthier and G. Tarjus, Phys. Rev. E **82**, 031502 (2010).

[20] N. W. Ashcroft, N. D. Mermin, and R. Smoluchowski, Solid state physics, 1977.

[21] M. Mézard and G. Parisi, J. Chem. Phys. **111**, 1076 (1999).

[22] G. Parisi and F. Zamponi, Rev. Mod. Phys. **82**, 789 (2010).

[23] A. Imhof and J. K. G. Dhont, Phys. Rev. Lett. **75**, 1662 (1995).

[24] A. Imhof and J. K. G. Dhont, Phys. Rev. E. **52**, 6345 (1995).

[25] A. J. Moreno and J. Colmenero, Phys. Rev. E. **74**, 021409 (2006).

[26] A. J. Moreno and J. Colmenero, J. Chem. Phys. **125**, 164507 (2006).

[27] Z. Zheng, F. Wang, and Y. Han, Phys. Rev. Lett. **107**, 065702 (2011).

[28] M. Letz, R. Schilling, and A. Latz, Phys. Rev. E **62**, 5173 (2000).

[29] R. Bose, R. Weiler, and P. Macedo, Phys. Chem. Glasses: Eur. J. Glass Sci. Technol. B **11**, 117 (1970).

[30] H. Tweer, N. Laberge, and P. Macedo, J. Am. Ceram. Soc. **54**, 121 (1971).

[31] S. W. Martin, J. Am. Soc. **74**, 1767 (1991).

[32] C. A. Angell, K. L. Ngai, G. B. McKenna, P. F. McMillan, and S. W. Martin, J. Appl. Phys. (2000).

[33] U. Bengtzelius, W. Gotze, and A. Sjolander, J. Phys. C **17**, 5915 (1984).

[34] S. Gottke, D. D. Brace, G. Hinze, and M. Fayer, J. Phys. Chem. B **105**, 238 (2001).

[35] T. R. Kirkpatrick and P. G. Wolynes, Phys. Rev. A **35**, 3072 (1987).

[36] T. Kirkpatrick, D. Thirumalai, and P. G. Wolynes, Phys. Rev. A: At. Mol. Opt. Phys. **40**, 1045 (1989).

[37] J.-P. Bouchaud and G. Biroli, J. Chem. Phys. **121**, 7347 (2004).

[38] G. Adam and J. H. Gibbs, J. Chem. Phys. **43**, 139 (1965).

[39] R. Monasson, Phys. Rev. Lett. **75**, 2847 (1995).

[40] T. R. Kirkpatrick and D. Thirumalai, Phys. Rev. Lett. **58**, 2091 (1987).

[41] A. Crisanti and H.-J. Sommers, Zeitschrift für Physik B Condensed Matter **87**, 341 (1992).

[42] A. Crisanti, H. Horner, and H.-J. Sommers, Zeitschrift für Physik B Condensed Matter **92**, 257 (1993).

[43] T. Castellani and A. Cavagna, J. Stat. Mech. Theor. Exp. **2005**, P05012 (2005).

[44] T. Gleim, W. Kob, and K. Binder, Phys. Rev. Lett. **81**, 4404 (1998).

[45] L. Berthier and W. Kob, J. Phys. Condens. Matter **19**, 205130 (2007).

[46] P. C. Martin, E. D. Siggia, and H. A. Rose, Phys. Rev. A **8**, 423 (1973).

[47] T. Maimbourg, J. Kurchan, and F. Zamponi, Phys. Rev. Lett. **116**, 015902 (2016).

[48] J. Kurchan, T. Maimbourg, and F. Zamponi, J. Stat. Mech. Theor. Exp. **2016**, 033210 (2016).

[49] Y. Brumer and D. R. Reichman, Phys. Rev. E **69**, 041202 (2004).

[50] L. Angelani, R. Di Leonardo, G. Ruocco, A. Scala, and F. Sciortino, Phys. Rev. Lett. **85**, 5356 (2000).

[51] M. D. Ediger, Annu. Rev. Phys. Chem. **51**, 99 (2000).

[52] E. V. Russell and N. Israeloff, Nature **408**, 695 (2000).

[53] R. Yamamoto and A. Onuki, Phys. Rev. Lett. **81**, 4915 (1998).

[54] R. Yamamoto and A. Onuki, Phys. Rev. E **58**, 3515 (1998).

[55] L. Berthier, G. Biroli, J.-P. Bouchaud, L. Cipelletti, and W. van Saarloos, *Dynamical heterogeneities in glasses, colloids, and granular media*volume 150 (OUP Oxford, 2011).

[56] L. Berthier, arXiv:1106.1739 (2011).

[57] L. Berthier *et al.*, Science **310**, 1797 (2005).

[58] G. Biroli, J.-P. Bouchaud, A. Cavagna, T. S. Grigera, and P. Verrocchio, Nat. Phys. **4**, 771 (2008).

[59] S. Karmakar, C. Dasgupta, and S. Sastry, PNAS **106**, 3675 (2009).

[60] G. M. Hocky, T. E. Markland, and D. R. Reichman, Phys. Rev. Lett. **108**, 225506 (2012).

[61] J. Russo and H. Tanaka, PNAS **112**, 6920 (2015).

[62] D. Chandler and J. P. Garrahan, Annu. Rev. Phys. Chem. **61**, 191 (2010).

[63] T. R. Kirkpatrick and D. Thirumalai, Phys. Rev. B **36**, 5388 (1987).

[64] K. N. Pham *et al.*, Science **296**, 104 (2002).

[65] T. Eckert and E. Bartsch, Phys. Rev. Lett. **89**, 125701 (2002).

[66] K. Pham *et al.*, EPL **75**, 624 (2006).

[67] T. Sentjabrskaja *et al.*, Soft Matter **9**, 4524 (2013).

[68] J. Hendricks, R. Capellmann, A. Schofield, S. Egelhaaf, and M. Laurati, Phys. Rev. E **91**, 032308 (2015).

[69] T. Voigtmann and J. Horbach, Phys. Rev. Lett. **103**, 205901 (2009).

[70] J. Bosse and Y. Kaneko, Phys. Rev. Lett. **74**, 4023 (1995).

[71] T. Voigtmann, EPL **96**, 36006 (2011).

[72] F. T. Nya, A. Ayadim, P. Germain, and S. Amokrane, J. Phys. Condens. Matter **24**, 325106 (2012).

[73] B. Schmid and R. Schilling, Phys. Rev. E **81**, 041502 (2010).

[74] A. Ikeda and K. Miyazaki, Phys. Lev. Lett. **104**, 255704 (2010).

[75] H. Jacquin and F. van Wijland, Phys. Rev. Lett. **106**, 210602 (2011).

[76] A. Crisanti and L. Leuzzi, Phys. Rev. Lett. **93**, 217203 (2004).

[77] A. Crisanti and L. Leuzzi, Phys. Rev. B **73**, 014412 (2006).

[78] A. Crisanti and L. Leuzzi, Phys. Rev. B **76**, 184417 (2007).

[79] A. Crisanti, L. Leuzzi, and M. Paoluzzi, Eur. Phys. J. E Soft Matter **34**, 1 (2011).

[80] C. Cammarota and G. Biroli, J. Chem. Phys. **138**, 12A547 (2013).

[81] W. Kob and L. Berthier, Phys. Rev. Lett. **110**, 245702 (2013).

[82] M. Ozawa, W. Kob, A. Ikeda, and K. Miyazaki, PNAS **112**, 6914 (2015).

[83] M. Dijkstra, R. van Roij, and R. Evans, Phys. Rev. E **59**, 5744 (1999).

[84] J. Bergenholtz and M. Fuchs, Phys. Rev. E **59**, 5706 (1999).

[85] K. Dawson *et al.*, Phys. Rev. E **63**, 011401 (2000).

[86] K. Dawson, G. Foffi, F. Sciortino, P. Tartaglia, and E. Zaccarelli, J. Phys. Condens. Matter **13**, 9113 (2001).

[87] G. Foffi, F. Sciortino, E. Zaccarelli, and P. Tartaglia, J. Phys. Condens. Matter **16**, S3791 (2004).

[88] P. Charbonneau, J. Kurchan, G. Parisi, P. Urbani, and F. Zamponi, J. Stat. Mech. Theor. Exp. **2014**, P10009 (2014).

[89] Y. H. Ikeda H, Miyazaki K and I. A, in preparation. .

[90] F. Faupel *et al.*, Rev. Mod. Phys. **75**, 237 (2003).

[91] C. Mayer *et al.*, Nat. Mater. **7**, 780 (2008).

[92] F. Hofling and T. Franosch, Rep. Prog. Phys. **76**, 046602 (2013).

[93] Y. Jin and P. Charbonneau, Phys. Rev. E **91**, 042313 (2015).

[94] J. Bosse and J. S. Thakur, Phys. Rev. Lett. **59**, 998 (1987).

[95] G. Brambilla *et al.*, Phys. Rev. Lett. **102**, 085703 (2009).

[96] S. P. Das, Rev. Mod. Phys. **76**, 785 (2004).

[97] M. Mézard and G. Parisi, Phys. Rev. Lett. **82**, 747 (1999).

[98] B. Coluzzi, M. Mézard, G. Parisi, and P. Verrocchio, J. Chem. Phys. **111**, 9039 (1999).

[99] B. Coluzzi, G. Parisi, and P. Verrocchio, J. Chem. Phys. **112**, 2933 (2000).

[100] I. Biazzo, F. Caltagirone, G. Parisi, and F. Zamponi, Phys. Rev. Lett. **102**, 195701 (2009).

[101] I. Biazzo, F. Caltagirone, G. Parisi, and F. Zamponi, J. Chem. Phys. **132**, 176101 (2010).

[102] H. Ikeda and A. Ikeda, arXiv:1603.06314 (2016).

[103] M. Goldstein, J. Chem. Phys. **51**, 3728 (1969).

[104] S. Sastry, P. G. Debenedetti, and F. H. Stillinger, Nature **393**, 554 (1998).

[105] Y.-L. Zhu and Z.-Y. Lu, J. Chem. Phys. **134**, 044903 (2011).

[106] M. Sellitto and F. Zamponi, EPL **103**, 46005 (2013).

[107] T. Obuchi, K. Takahashi, and K. Takeda, J. Phys. A **43**, 485004 (2010).

[108] T. Shikata, Chem. Eng. Sci. **56**, 2957 (2001).

[109] N. Koumakis and G. Petekidis, Soft Matter **7**, 2456 (2011).

[110] H. Yoshino and F. Zamponi, Phys. Rev. E **90**, 022302 (2014).

[111] T. Morita and K. Hiroike, Prog. of Theor. Phys. **25**, 537 (1961).

[112] M. Ozawa and L. Berthier, arXiv:1609.07979 (2016).

[113] W. Greiner, L. Neise, and H. Stöcker, *Thermodynamics and statistical mechanics* (Springer Science & Business Media, 2012).